Title
Calcium-Activated Chloride Channels (CaCCs) regulate action potential and synaptic responses in hippocampal pyramidal neurons

Author
Huang, Wendy C.

Publication Date
2010

Peer reviewed|Thesis/dissertation

Calcium-Activated Chloride Channels (CaCCs) regulate action potential and synaptic responses in hippocampal pyramidal neurons

by

Wendy C. Huang

DISSERTATION

Submitted in partial satisfaction of the requirements for the degree of

DOCTOR OF PHILOSOPHY

in

NEUROSCIENCE

in the

GRADUATE DIVISION

of the

UNIVERSITY OF CALIFORNIA, SAN FRANCISCO

[redacted]

ACKNOWLEDGMENTS

First I thank my thesis advisor, Lily Jan, for her unfailing support and patient teaching, and for allowing me to join her lab and learn from her. In the past few years I have benefited enormously from her big-picture perspectives, systematic thinking, meticulous editing, subtle yet effective leadership, good humor and calming presence, as she showed me the ropes and guided me through difficult scientific concepts, hard experiments, qualifying exams, thesis meetings, research talk preps, and manuscript preparations, just to name a few. It is hard to thank her enough for all that she has done during my scientific training.

I thank my thesis committee, Roger Nicoll, Yuriy Kirichok, Michael Stryker, and my thesis advisor, Lily Jan, for guiding me through the experiments and pushing me to tackle scientific problems with both the simplest and the most powerful experiments. I thank Roger for brainstorming experiments with me, especially the ones illuminating physiological functions of channels at or near the synapses. I thank Yuriy for teaching me to 1) tackle "important problems" and 2) to use the most "direct and reliable methods" to solve them. I thank Michael for rallying the committee every thesis committee meeting to set new time tables for my experiments so I can quickly move on to the next stage.

I thank my labmates in the Jan Lab for their friendship and support as I struggle and fumble in my training. Among them I thank Kimberly Raab-Graham and Patrick Haddick for letting me tag along as a beginning student, on a project that I failed to pursue due to inexperience. I thank Jim Berg for initiating me into a project that eventually turned into this thesis work. I thank Woo-Ping Ge for teaching me all I know

about electrophysiology rig work and for being a wise and supportive rigmate throughout the years. I thank Shaohua Xiao for showing me how to culture neurons and to work with shRNAs and I thank Fen Huang for providing the methods for the molecular parts of this work. I thank Shi-Bing Yang and Huanghe Yang for gleaning incisive scientific insights from my recordings and for making this work more solid with every conversation. I thank Jill Wildonger, Quan Yuan, and Peter Soba for helping out with figure-making during the days of manuscript and thesis preparation, and for their kind words of encouragement. I thank Desiree Thayer for being a great friend, for being there whenever I needed someone to hear me out. I also thank Hye Young Lee, Jason Tien, Josh Bagley, Xiu Ming Wong, and David Gorczyca for being wonderful friends, and for putting up with me all this time.

I thank Barry Connors and David Pinto for taking me in during college and opening my eyes to scientific research; without them I would not be in graduate school today.

My personal development gained dimensions from friendships outside of the lab. I thank Thu Trinh, Iwalani Kaya, Suzanne Delaney, Sandy Hazanow, Emily Hipp, Roena Lim and Dana Bache, and Carolyn Whitney for all the good laughs and good fun we've had both during and off snowboarding season.

I thank Diana Sisneros for her unwavering faith in me and for always watching out for me.

Lastly and importantly, I thank my parents and my sister for their unconditional support, allowing me to freely pursue all that life has to offer.

Lily Y. Jan directed and supervised the research that forms the basis for this dissertation. Wendy C. Huang performed all of the experiments and analyses presented in this dissertation except for Figure 6 of Chapter 2 which was done by collaborators Fen Huang and Shaohua Xiao. shRNA construct testing and packaging was done in collaboration with Shaohua Xiao. This work is comparable to work for a standard thesis awarded by the University of California, San Francisco.

Lily Yeh Jan

Calcium-Activated Chloride Channels (CaCCs) regulate action potential and synaptic responses in hippocampal pyramidal neurons

by

Wendy C. Huang

ABSTRACT

Neurons rely on action potentials for propagating signals and synaptic potentials for responding to other neurons. The calcium influx during these electrical events opens calcium-activated ion channels for feedback regulation. Here we identify calcium-activated chloride channels (CaCCs) to be a novel mechanism of calcium-dependent feedback regulation in hippocampal neurons. We provide the first evidence that CaCCs are present in these neurons and demonstrate that CaCCs are activated during neuronal signaling to shorten action potentials and dampen excitatory synaptic potentials. Having recently identified TMEM16A and TMEM16B as CaCCs, we further show that TMEM16B but not TMEM16A is important for hippocampal CaCC, thus laying the groundwork for deciphering the dynamic CaCC modulation of neuronal signaling in hippocampal neurons important for learning and memory.

TABLE OF CONTENTS

LIST OF FIGURES

Chapter 1 Introduction

Action potential firing and synaptic transmission are fundamental processes underlying neuronal signaling. Neurons use action potentials to propagate signals they receive to their nerve terminals to induce transmitter release. The magnitude of the synaptic potentials generated by neurotransmitters determines the likelihood for action potential initiation in the postsynaptic neuron. The waveform of the action potential in turn influences the firing pattern. Given that information about the external sensory world and the internal mental state is encoded in the frequency and firing pattern of action potentials, it is important to understand the basis for the generation and modulation of these neuronal signals.

Investigation over several decades has identified the basic ion channels contributing to both action potential firing and synaptic transmission and revealed that both involve Ca^{2+} influx that can activate Ca^{2+}-activated channels for modulation. It remains an open question whether calcium-activated chloride channels (CaCCs) are activated during action potential or synaptic potentials in hippocampal pyramidal neurons and, if so, how CaCC activity may modulate neuronal signaling.

In action potential firing, voltage-activated Na^+ and K^+ channels make up the basic machinery for the generation of an action potential (Hodgkin and Huxley, 1952). By now we have learned that during an action potential the membrane depolarization activates voltage-gated Ca^{2+} channels and the resulting Ca^{2+} influx activates the big-conductance Ca^{2+}-activated K^+ channels (BK) and the small-conductance Ca^{2+}-activated K^+ channels (SK) (Fakler and Adelman, 2008). These Ca^{2+}-activated K^+ channels in turn

modulate spike waveform such as action potential duration and afterpotentials (Adams et al., 1982; Lancaster and Nicoll, 1987; Storm, 1987a, b). For example, BK channels are known to be present in both soma and axon terminals of hippocampal pyramidal neurons and can regulate spike duration in both locations. Whereas BK channels controlling spike duration in the axon terminal modulate the neurotransmitter release (Hu et al., 2001; Lingle et al., 1996; Petersen and Maruyama, 1984; Raffaelli et al., 2004; Robitaille et al., 1993), BK channels affecting the spike duration near the soma control the firing pattern (Madison and Nicoll, 1984; Shao et al., 1999).

Further out from the soma, excitatory synaptic transmission occurring on dendrites involves glutamatergic α-amino-3-hydroxy-5-methyl-4-isoxazolepropionic acid receptors (AMPA-Rs) and N-methyl D-aspartate receptors (NMDA-Rs). Here Ca^{2+} ions entering the cell via NMDA receptors activate Ca^{2+}-activated K^+ channels that in turn shape synaptic responses and influence synaptic plasticity (Lin et al., 2008; Ngo-Anh et al., 2005; Stackman et al., 2002). For example, SK channels activated by Ca^{2+} flowing through NMDA receptors during an excitatory postsynaptic potential (EPSP) serve as a brake on excitatory synaptic transmission by dampening the size of the synaptic response and reducing the likelihood of LTP induction (Hammond et al., 2006; Stackman et al., 2002).

Whereas Ca^{2+}-activated K^+ channels have well-established physiological functions, with the BK channels contributing to spike repolarization and the SK channels modulating synaptic transmission and plasticity in hippocampal pyramidal neurons, it is currently unknown whether and how Ca^{2+}-activated Cl^- channels (CaCCs) are involved in these fundamental processes. Indeed, even the basic question regarding the existence of

CaCCs in hippocampal pyramidal neurons has yet to be addressed, notwithstanding earlier studies establishing the presence of CaCCs in anterior pituitary neurons (Korn et al., 1991), amygdale neurons (Sugita et al., 1993) and cingulated cortical neurons (Higashi et al., 1993).

Part of the reason for the paucity of information regarding CaCCs in central neurons may be attributed to the lack of specific blockers and the uncertainty regarding their molecular identity. Whereas earlier molecular candidates for CaCC have not recapitulated the distribution and channel properties characteristic of CaCC, three recent studies with different approaches have reached the same conclusion that TMEM16A of a family of transmembrane protein with unknown functions encodes a CaCC (Caputo et al., 2008; Schroeder et al., 2008; Yang et al., 2008). In addition to TMEM16A, TMEM16B also gives rise to CaCC current that has the properties of classical CaCC (Pifferi et al., 2009; Schroeder et al., 2008).

Recent genetic studies have shown that TMEM16A is important for vasoconstriction in the lung (Manoury et al., 2010), airway surface liquid maintenance (Rock et al., 2009), rhythmic contraction in the gastrointestinal tracts (Huang et al., 2009; Hwang et al., 2009), and fluid excretion in salivary gland cells (Romanenko et al., 2010). Recent molecular studies further indicate that TMEM16B likely corresponds to the CaCC that mediates high-gain, low-noise amplification of odorant signals in olfactory sensory neurons (Stephan et al., 2009) and feedback regulation of photoreceptor terminals (Barnes and Hille, 1989; Stohr et al., 2009).

With these recent developments in the molecular studies of CaCCs, it is timely to address the long-standing open question whether there are CaCCs in the hippocampal

pyramidal neurons, a class of mammalian neurons that have been extensively characterized as a model system for physiological analyses of action potential and synaptic potential generation, to lay the ground work for the exploration of the physiological contributions of Ca^{2+}-activated Cl^- channels to neuronal signaling in the mammalian brain. In this study, we find that CaCCs are present in hippocampal pyramidal neurons and can be activated by Ca^{2+} influx through voltage-gated Ca^{2+} channels to shorten action potential duration. We further show that CaCCs are also in close vicinity of NMDA-Rs on dendrites so that their activation provides a brake to the NMDA-R mediated synaptic response. Moreover, we report that TMEM16B but not TMEM16A is important for the CaCC in hippocampal pyramidal neurons.

Chapter 2 Evidence of CaCCs in Hippocampal Neurons

Activating voltage-gated Ca^{2+} channels by depolarizing hippocampal pyramidal neurons induces a tail current that is carried by Cl^- ions

Previous studies of smooth muscles and DRG neurons have shown that activation of voltage-gated Ca^{2+} channels could lead to the activation of Ca^{2+}-activated Cl^- channels (Frings et al., 2000; Scott et al., 1995). To look for evidence for the presence of CaCC activity in hippocampal pyramidal neurons, we therefore applied a 200 ms depolarization step from -70 mV holding potential to 0 mV to activate voltage-gated Ca^{2+} channels. This depolarizing prepulse resulted in Ca^{2+} influx due to the large inward Ca^{2+} current occurring during the prepulse depolarization, and was followed by a slow tail current (arrow, Figure 1A) that was readily detected in DIV 14 cultured pyramidal neurons and also in CA1 pyramidal neurons of acute slices from P14-21 mice.

Only Ca^{2+} and Cl^- ions are possible charge carriers in these experiments because 1) Na^+ was replaced by NMDG and Na^+ channels were blocked by TTX; and 2) K^+ ions were removed and K^+ channels were blocked with Cs^+ and TEA in the internal solution and 4AP in the external solution, which also included the $GABA_A$ receptor antagonist picrotoxin. For the traces shown in Figure 1A, 23 mM Cl^- was included in the internal solution, with an expected E_{Cl} of – 46.8 mV so that activation of Cl^- channels would result in an inward current.

To verify that Cl^- is the ion carrier for the tail current, we tested three different internal Cl^- concentrations, 5 mM, 10 mM, and 23 mM, and determined the reversal

potential of the slow tail current by bringing the membrane potential following the prepulse depolarization to different levels to vary the driving force for the tail current. The voltage steps following the prepulse depolarization ranged from -100 mV to -25 mV (5 or 10 mV steps), encompassing the range of Cl^- driving forces for both inward and outward Cl^- fluxes. After subtracting the background current elicited without a depolarization prepulse (-70 mV holding without 0 mV depolarization prepulse) from the tail current elicited with a depolarization prepulse (to 0 mV), we measured the average current amplitude at each voltage step at 150-200 ms after the end of the 0 mV depolarization prepulse, and plotted this tail current as function of voltage to determine the reversal potential where the tail current reversed its direction (Figure 1B).

We found that the reversal potential, plotted as a function of $\log_{10}[Cl^-]_{in}$, followed the Nernst equation with a slope of 58 mV (Figure 1C). Hence this tail current following Ca^{2+} channel activation reversed at the E_{Cl} and changed its reversal potential accordingly as the internal Cl^- concentration was altered. These results reveal that this tail current observed in the hippocampal pyramidal neurons is a Cl^- current.

The tail current is activated by Ca^{2+}

In order to verify that this tail Cl^- current requires Ca^{2+} for its activation, we applied different levels of prepulse depolarization ranging from -70 mV (no depolarization) to +100 mV (closer to the estimated E_{Ca}). If the tail current is a Ca^{2+} activated current, depolarizing towards E_{Ca} thereby reducing the driving force for net Ca^{2+} influx ought to lead to smaller tail current. As seen in the example in Figure 2A, the tail current elicited by a depolarization prepulse of 0 mV (black) is larger than the tail

current elicited by a prepulse of +40 mV (red). We further plotted the tail current amplitude as a function of different prepulse voltages (n = 52, Figure 2B). At prepulse potentials more negative than - 30 mV Ca^{2+} influx was minimal due to insufficient activation of the voltage-gated Ca^{2+} channels and consequently there was little tail current. Further depolarization during the prepulse gave rise to larger tail current, until a maximum was reached near 0 mV prepulse (n = 52, Figure 2B). As the prepulse depolarization approached E_{Ca} (calculated to be > 100 mV), the tail current diminished in size, suggesting that the tail current amplitude correlates with the size of the Ca^{2+} influx.

If Ca^{2+} is responsible for tail current activation, prolonging the prepulse depolarization that causes Ca^{2+} influx should increase the amplitude of the tail current. As shown in Figure 2C, the tail current following a 100 ms depolarization prepulse to 0 mV (top trace) was much smaller than the tail current following a 500 ms depolarization prepulse to 0 mV (bottom trace). We further tested the prepulse durations of 200 ms and 1000 ms. While the tail current increased in size in response to longer 0 mV prepulses (n = 22, $p < 0.01$, Figure 2D, blue bars), the tail current size remained unchanged for the +100 mV prepulses regardless of their duration (n = 22, p = 0.9, Figure 2D, black bars). Unlike lengthening a 0 mV prepulse depolarization which prolongs Ca^{2+} influx and therefore increases the tail current, prolonging +100 mV depolarization prepulse does not affect the tail current size because the driving force for net Ca^{2+} influx is greatly reduced at +100 mV regardless of the prepsulse duration (net Ca^{2+} flux is minimal near E_{Ca}).

To further verify that the tail current requires Ca^{2+} influx, we replaced external Ca^{2+} with Ba^{2+} (Figure 3A, red) – which goes through the voltage-activated Ca^{2+} channels even better than Ca^{2+} – and found tail current nearly eliminated (1.9 ± 0.09% of

control, n = 13, $p < 0.01$, Figure 3A, red). Thus, Ca^{2+}, but not Ba^{2+}, can activate the tail current (Figure 3A, black). Next we included 10 mM BAPTA in the whole cell patch pipette solution to chelate Ca^{2+}, and found that the tail current was nearly abolished (Figure 3B, red, 2.1 ± 0.02% of control in black, n = 12, $p < 0.01$). Taken together, these experiments show that the tail current is a Ca^{2+}-activated Cl^- current.

The tail current is blocked by CaCC blockers and reduced by shRNA knockdown of TMEM16B

Having found that the tail current following Ca^{2+} channel activation is a Ca^{2+}-activated Cl^- current, we next tested two classical CaCC blockers, niflumic acid (NFA) and 5-nitro-2-(3-phenylpropylamino)benzoic acid (NPPB). Whereas a depolarization from -70 mV to 0 mV resulted in an inward Ca^{2+} current followed by a tail current (tail current measured at -90 mV, E_{Cl} = - 46.8 mV), both NFA and NPPB significantly reduced the tail current while leaving the inward Ca^{2+} current intact (NFA 28 ± 5.1% of control, n = 9, $p < 0.001$; NPPB 18 ± 5.9 % of control, n = 10, $p < 0.001$) (Figures 4A-4D), providing further support that the tail current is a Ca^{2+}-activate Cl^- current.

To test whether hippocampal CaCC requires TMEM16A, we compared CA1 pyramidal neurons in hippocmpal slices from wildtype (n = 7) and TEMEM16A KO mice (n = 11) and found no significant difference in the tail current (109 ± 9% of control with 0 mV prepulse, $p = 0.9$) (Figure 5A). Therefore TMEM16A is not required for the CaCC in hippocampal pyramidal neurons.

Because TMEM16B from the same TMEM16 family of proteins with eight transmembrane segments also gives rise to CaCC (Pifferi et al., 2009; Schroeder et al.,

2008) and we have found TMEM16B mRNA in these hippocampal neurons (Figures 6A-6D), we used two different shRNA constructs to knock down TMEM16B, and tested their effects on the tail current. Infecting cultured hippocampal neurons with lentivirus encoding green fluorescence protein (GFP) and either shRNA #2 or shRNA #5 for TMEM16B knockdown, or scrambled RNA as control, we found that, while the infected neurons expressing either shRNA displayed normal inward Ca^{2+} current during prepulse depolarization compared to scrambled control (shRNA #2, 104 ± 12%, n =18, p = 0.2, shRNA #5, 101 ± 18%, n = 12, p = 0.3, Figures 5B and 5C), shRNA #2 or shRNA #5 knockdown of TMEM16B significantly reduced the tail current amplitude by 60 ± 4.5% and 61 ± 5%, respectively (scrambled, n = 17, shRNA #2, n = 18, $p < 0.01$, shRNA #5, n = 12, $p < 0.01$, 12 days after infection, Figures 5B and 5C). These findings indicate that TMEM16B is important for the generation of hippocampal CaCC.

Figure 1

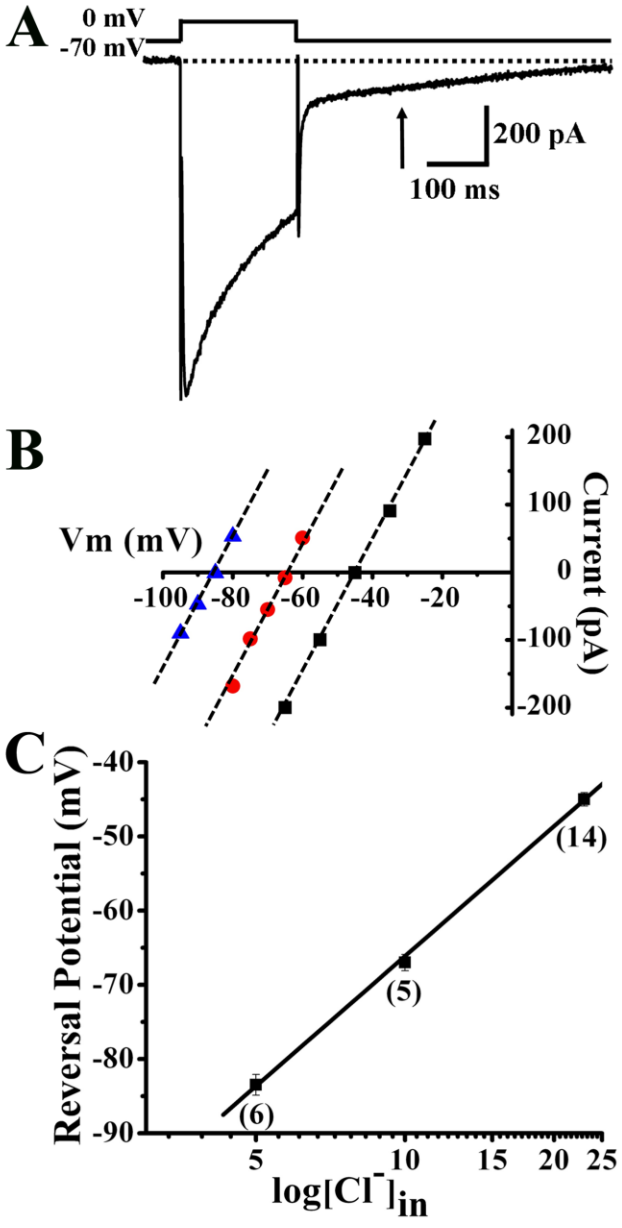
A
0 mV
-70 mV
200 pA
100 ms
B
Vm (mV)
-100
-80
-60
-40
-20
200
100
0
-100
-200
Current (pA)
C
Reversal Potential (mV)
-40
-50
-60
-70
-80
-90
(14)
(5)
(6)
5
10
15
20
25
log[Cl-]in

Figure 1. The tail current induced by Ca^{2+} channel activation in hippocampal pyramidal neurons is a Cl^- current

(A) Depolarizing hippocampal pyramidal neurons to 0 mV results in voltage-activated Ca^{2+} current followed by a long tail current (cultured neurons: n = 39, 104 ± 8.9 pA, acute slices: n = 33, 115 ± 7.3 pA). Arrow points at the 150-200 ms time window at which the tail current amplitude was taken.

(B) The reversal potential of the long tail current changes with internal Cl^- concentrations in accordance with Nernst equation. Plotted are current-voltage relations of tail current recorded using 3 different internal Cl^- concentrations (black, 23 mM Cl^-_{in}, red, 10 mM Cl^-_{in}, blue, 5 mM Cl^-_{in}. The calculated E_{Cl} is – 46.8 mV for 23 mM Cl^-_{in}, - 67.8 mV for 10 mM Cl^-_{in}, and -85.3 mV for 5 mM Cl_{in}).

(C) In hippocampal pyramidal neurons the slow tail current following Ca^{2+} channel activation reverses at E_{Cl}. Number in parenthesis indicates number of recordings.

Figure 2

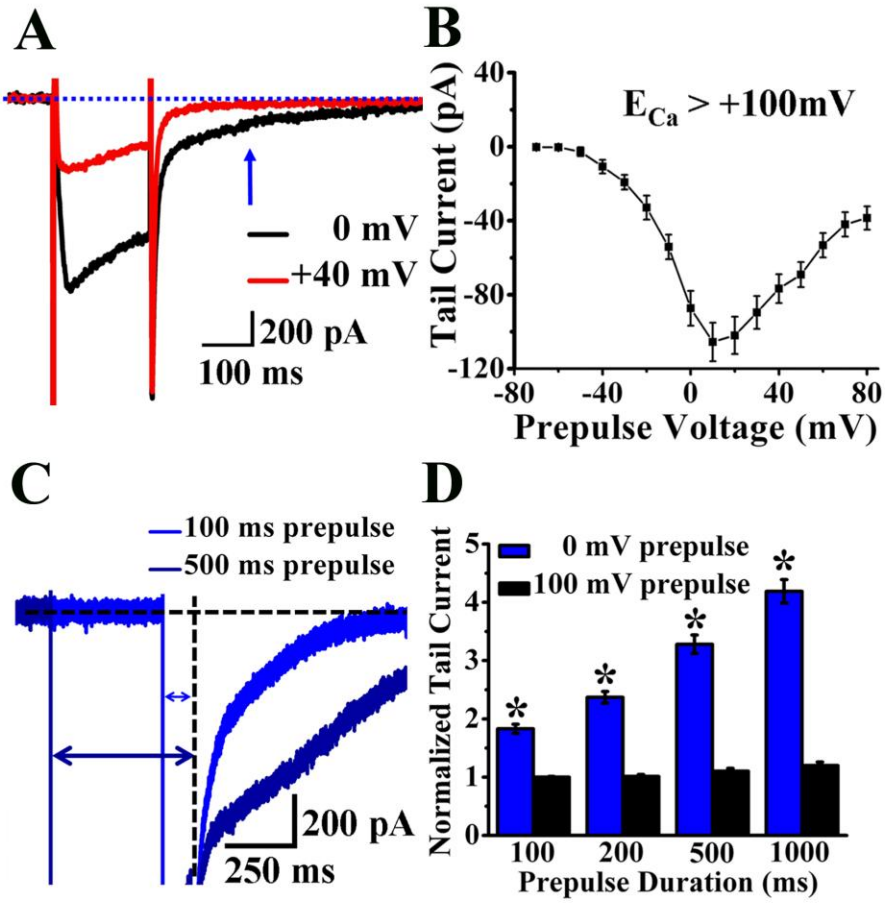
A
0 mV
+40 mV
200 pA
100 ms
B
E_{Ca} > +100mV
Tail Current (pA)
40
0
-40
-80
-120
-80
-40
0
40
80
Prepulse Voltage (mV)
C
100 ms prepulse
500 ms prepulse
200 pA
250 ms
D
0 mV prepulse
100 mV prepulse
Normalized Tail Current
5
4
3
2
1
0
100
200
500
1000
Prepulse Duration (ms)

Figure 2. The tail current in hippocampl pyramidal neurons requires calcium

(A) Tail current elicited by a depolarization prepulse to 0 mV (black) is larger than the tail current elicited by a prepulse to + 40 mV (red). Blue arrow points at the 150-200 ms time window at which the tail current amplitude was taken.

(B) Tail current diminishes in amplitude as prepulse voltage approaches the reversal potential of Ca^{2+} (estimated $E_{Ca} > +100$ mV) resulting in reduced driving force for Ca^{2+} influx ($n = 52$).

(C) Tail current is larger when the 0 mV prepulse is lengthened (top trace, shorter arrows, 0 mV depolarization for 100 ms; bottom trace, longer arrows, 0 mV depolarization for 500 ms).

(D) While the tail current increases in size with longer 0 mV prepulse depolarization (blue, $n = 22$, $p < 0.01$), the size of tail current following +100 mV prepulse (near E_{Ca}) remains unchanged regardless of duration (black, $n = 22$, $p = 0.9$).

Figure 3

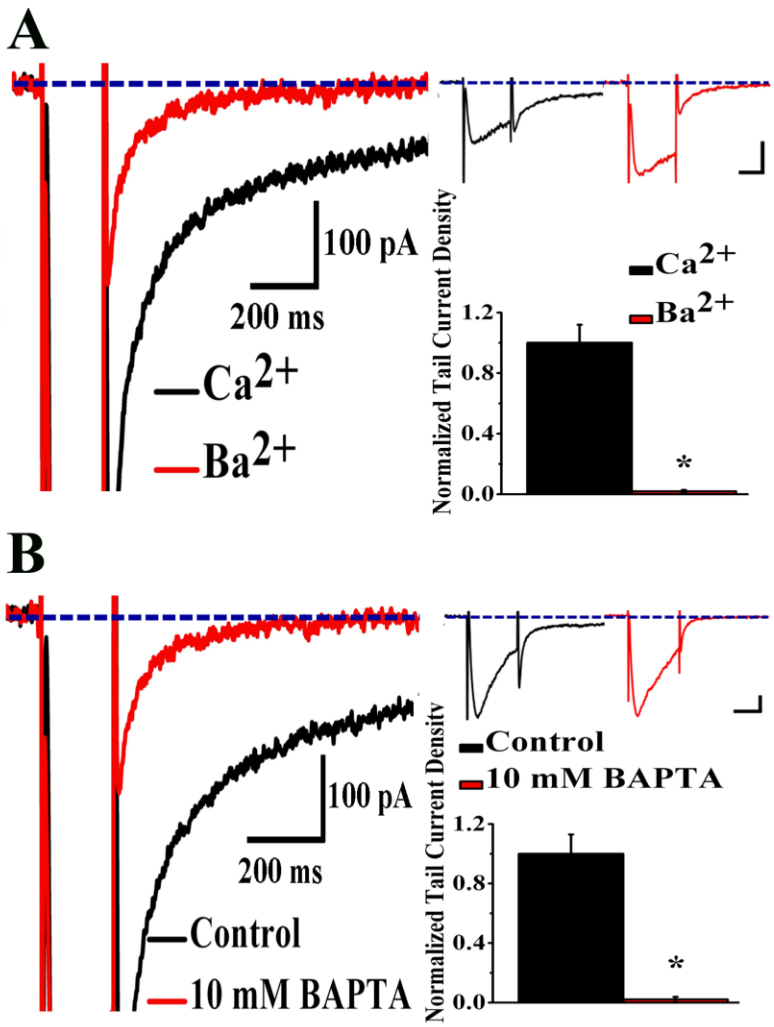
A
100 pA
200 ms
Ca2+
Ba2+
Normalized Tail Current Density
Ca2+
Ba2+
1.2
0.8
0.4
0.0
*
B
100 pA
200 ms
Control
10 mM BAPTA
Normalized Tail Current Density
Control
10 mM BAPTA
1.2
0.8
0.4
0.0
*

Figure 3. The tail current in hippocampl pyramidal neurons is a Ca^{2+}-activated Cl^- current

(A) Replacing external Ca^{2+} with Ba^{2+} removes the tail current (red). Ba^{2+} ions can go through voltage-gated Ca^{2+} channels and carry the inward current (right top, red), but cannot activate Cl^- tail current. The Cl^- tail current requires Ca^{2+} for activation (black) ($n = 13$, $p < 0.01$). Scale bar for right top panel, 100 ms, 200 pA.

(B) 10 mM BAPTA in the pipette solution eliminates tail current (left) while leaving the inward Ca^{2+} current intact (right top, red). The Cl^- tail current requires Ca^{2+} for activation (black) ($n = 12$, $p < 0.01$). Scale bar for right top panel, 100 ms, 200 pA.

Figure 4

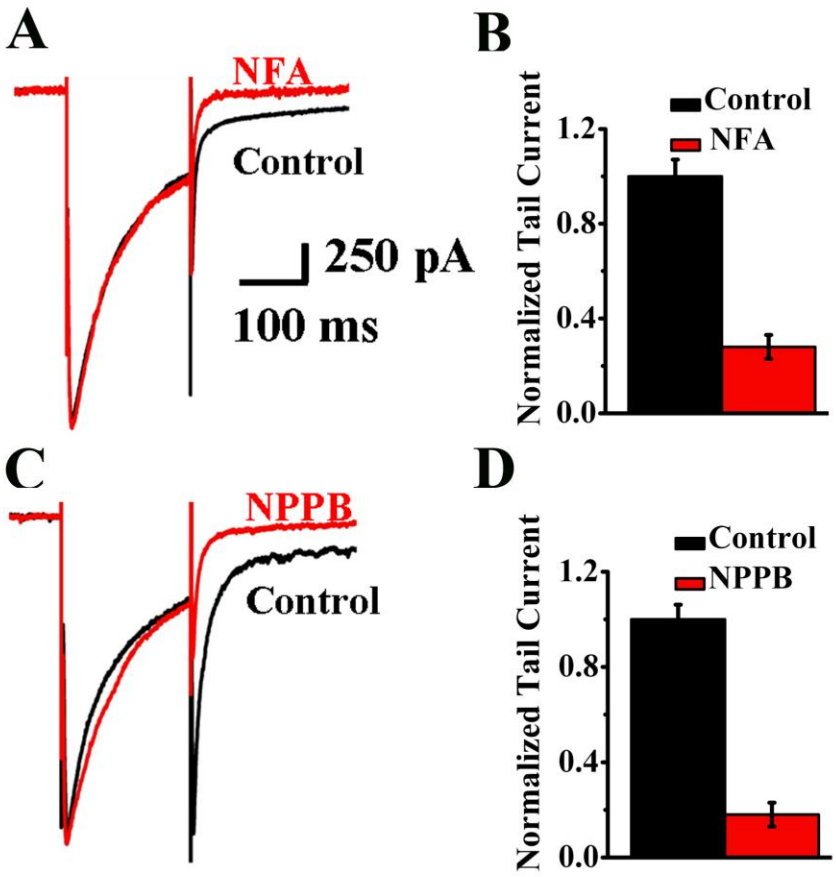
A
NFA
Control
250 pA
100 ms
B
Control
NFA
Normalized Tail Current
1.2
0.8
0.4
0.0
C
NPPB
Control
D
Control
NPPB
Normalized Tail Current
1.2
0.8
0.4
0.0

Figure 4. Ca^{2+}-activated Cl^- current in hippocampal pyramidal neurons is sensitive to two different CaCC blockers

Ca^{2+}-activated Cl^- current in cultured hippocampal pyramidal neurons is significantly reduced by two different CaCC blockers, (A-B) 100 μM NFA (28 ± 5.1% of control, n = 9, $p < 0.001$) and (C-D) 100 μM NPPB (18 ± 5.9% of control, n = 10, $p < 0.001$).

Figure 5

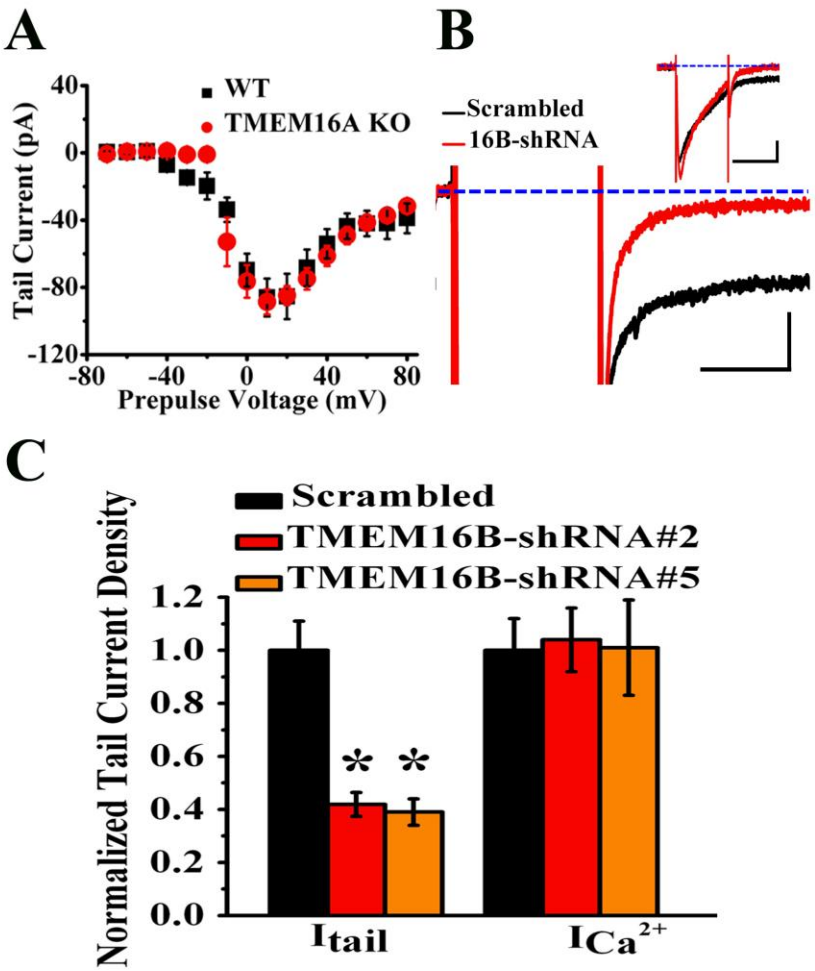
A
B
C
WT
TMEM16A KO
Tail Current (pA)
Prepulse Voltage (mV)
Scrambled
16B-shRNA
Scrambled
TMEM16B-shRNA#2
TMEM16B-shRNA#5
Normalized Tail Current Density
Itail
ICa2+

Figure 5. Ca^{2+}-activated Cl^- current in hippocampal pyramidal neurons is sensitive to two different CaCC blockers and is reduced by TMEM16B shRNA knockdown, but is still present in TMEM16A knockout mice

(A) Ca^{2+}-activated Cl^- current is still present in hippocampal slices from TMEM16A knockout mice (wildtype, n = 7, TMEM16A knockout, n = 11, p = 0.9).

(B) Ca^{2+}-activated Cl^- current in cultured hippocampal pyramidal neurons is significantly reduced by TMEM16B shRNA knockdown (red), but not by scrambled RNA control (black). Inset (top right): whereas the Ca^{2+}-activated Cl^- current is reduced by shRNA knockdown, the Ca^{2+} current is unaffected. Scale bar, 100 ms, 100 pA.

(C) Ca^{2+}-activated Cl^- current is reduced by 60 ± 4.5% and 61 ± 5%, respectively, by two different TMEM16B shRNA, #2 and #5 (scrambled, n = 17, shRNA #2, n = 18 , $p < 0.01$, shRNA #5, n = 12, $p < 0.01$, 12 days after infection). Voltage-activated Ca^{2+} current remains intact in neurons infected with TMEM16B shRNAs (shRNA #2, p = 0.2, shRNA #5, p = 0.3).

Figure 6

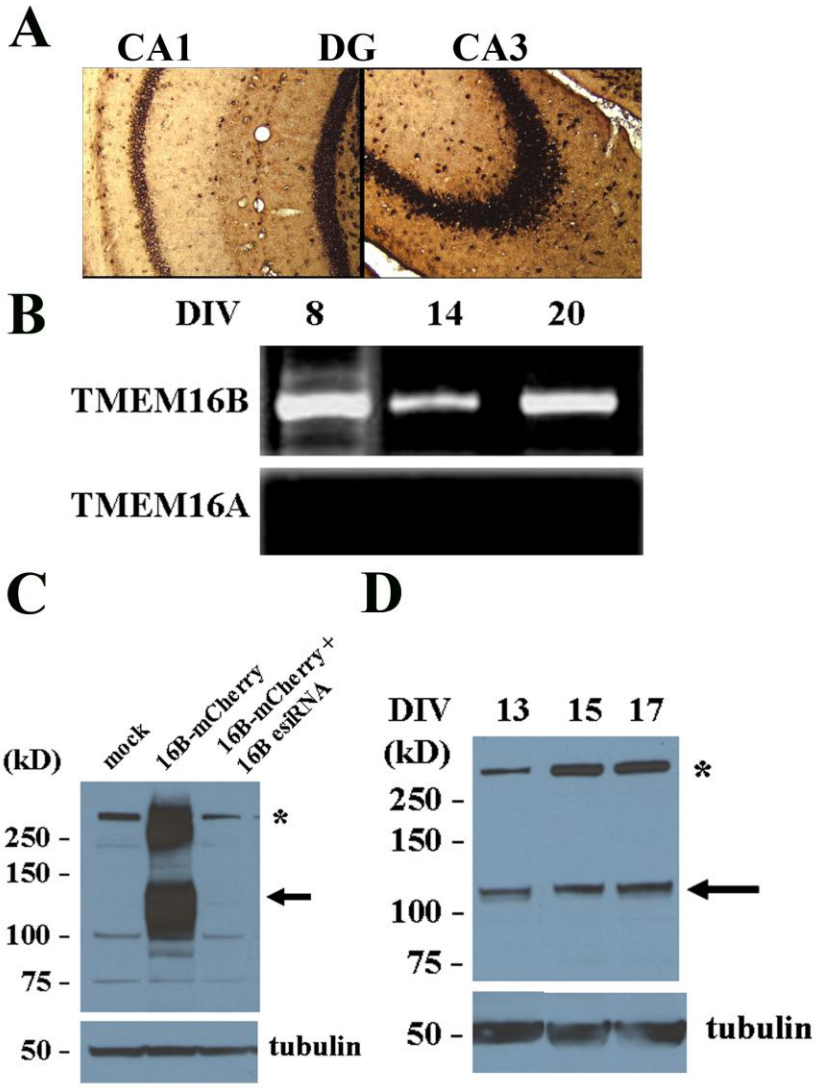
A
CA1
DG
CA3
B
DIV
8
14
20
TMEM16B
TMEM16A
C
(kD)
mock
16B-mCherry
16B-mCherry+
16B esiRNA
250 -
150 -
100 -
75 -
50 -
*
tubulin
D
DIV
13
15
17
(kD)
250 -
150 -
100 -
75 -
50 -
*
tubulin

Figure 6. TMEM16B is expressed in hippocampal pyramidal neurons

(A) TMEM16B mRNA expression in mouse hippocampus is revealed by *in situ* hybridization, showing strong TMEM16B signals in dentate granule cells, hilar interneurons, and CA1 pyramidal neurons (left) and CA3 pyramidal neurons (right).

(B) TMEM16B mRNA in cultured hippocampal neurons is revealed by RT-PCR. TMEM16B (top), but not TMEM16A (bottom), is expressed in neurons 8, 14, and 20 days *in vitro* (DIV) (left to right). PCR products were confirmed to be TMEM16B.

(C) Rabbit polyclonal antibody against TMEM16B recognized the exogenously expressed TMEM16B-mCherry in HEK293 cells. Cotransfection of TMEM16B-mCherry wth 16B esiRNA to knock down TMEM16B expression (the right most lane) dramatically reduced the expression of TMEM16B-mCherry in HEK293 cells. Bottom arrow points to 132 kD, the molecular weight of TMEM16B-mCherry. The heavier band of about twice the molecular weight is possibly a dimer of TMEM16B-mCherry. * indicates non-specific signal due to antibody cross-reactivity. Bottom panel is tubulin loading control.

(D) TMEM16B protein is detected in cultured hippocampal neuron 13, 15, and 17 DIV by western blot. Bottom arrow points to the band for TMEM16B. * indicates a non-specific band. Bottom panel is tubulin loading control.

Chapter 3 CaCC modulation of action potential

The action potential in hippocampal pyramidal neurons is broadened by CaCC blockers and by shRNA knockdown of TMEM16B

To assess whether CaCC regulates action potentials in hippocampal neurons, we applied a brief, 2 ms current injection (just above threshold to elicit a spike 90% of the time) to elicit a single action potential every 20 seconds, and tested for the effect of NFA and NPPB. As shown in Figure 1A with representative action potential traces in control solution before NFA application (black), after application of NFA (red), and then after washout of NFA (blue), NFA caused spike broadening; there was a dose-dependent increase of the spike width as function of $\log_{10}$[NFA] (Figure 1B) (spike width measured at 33% of the peak of the spike and then normalized to that measured in control solution). Similar results were obtained with a second CaCC blocker, NPPB (Figures 1C and 1D). The finding that two structurally distinct CaCC blockers, NFA and NPPB, cause action potential broadening in a reversible manner with high potency ($IC_{50} < 5$ μM) suggests that CaCC controls action potential repolarization.

To verify that the spike broadening is due to blocking CaCC, we tested for the effect of removing external Ca^{2+}. Removal of external Ca^{2+} caused action potential broadening, indicating that Ca^{2+} influx during the action potential is important for controlling spike duration. Moreover, NFA application in external solution without Ca^{2+} caused no further broadening of action potential (103 ± 2.7 %, n = 8, p = 0.4, Figure 2). The occlusion of NFA effect by the removal of Ca^{2+} further supports the notion that the NFA broadens the action potential by blocking Ca^{2+}-activated Cl^- channels.

Given that shRNA knockdown of TMEM16B reduced Ca^{2+}-activated Cl^- current induced by Ca^{2+} influx through voltage-gated Ca^{2+} channels (chapter 2, Figures 5B and 5C), we asked whether TMEM16B-CaCC affects spike waveform. Indeed, knockdown of TMEM16B by shRNA #2 or shRNA #5, but not the scrambled control RNA, lengthened the spike duration by 50 ±7.6% and 40 ± 5.2% respectively (scrambled, 2.3 ± 0.098 ms, n = 11, shRNA #2, 3.4 ± 0.018 ms, n = 9, $p < 0.001$, shRNA #5 3.2 ± 0.023 ms, n = 7, $p < 0.001$) (Figures 3A and 3B). These results suggest that TMEM16B-CaCC in hippocampal pyramidal neurons shortens action potential duration by facilitating repolarization.

CaCC shortens action potentials in CA3 pyramidal neurons without affecting transmitter release from their axon terminals

As shown in Figures 4 and 5, blocking CaCC caused spike broadening in both CA1 and CA3 pyramidal neurons in hippocampal slices (CA1, 144 ± 2%, n = 10, $p < 0.05$, CA3, 158 ± 5.6%, n = 10, $p < 0.005$). Moreover, the spike broadening persisted in the presence of calcium/calmodulin activated kinase II (CaMKII) inhibitor KN62 (CA1, 139 ± 9%, n = 9, $p < 0.005$, CA3, 150 ± 8%, n = 11, $p < 0.005$, Figure 4B, right), indicating that CaMKII is not required for Ca^{2+} activation of CaCC to regulate the action potential waveform. Whereas 10 mM BAPTA in the internal solution prevented CaCC activation following the opening of voltage-gated Ca^{2+} channels (chapter 2, Figure 3), NFA still caused action potential broadening when 10 mM EGTA was included in the internal solution (143 ± 2%, n = 5, $p < 0.001$, Figure 4B), indicating that CaCCs are in close vicinity of voltage-gated Ca^{2+} channels.

Figure 1

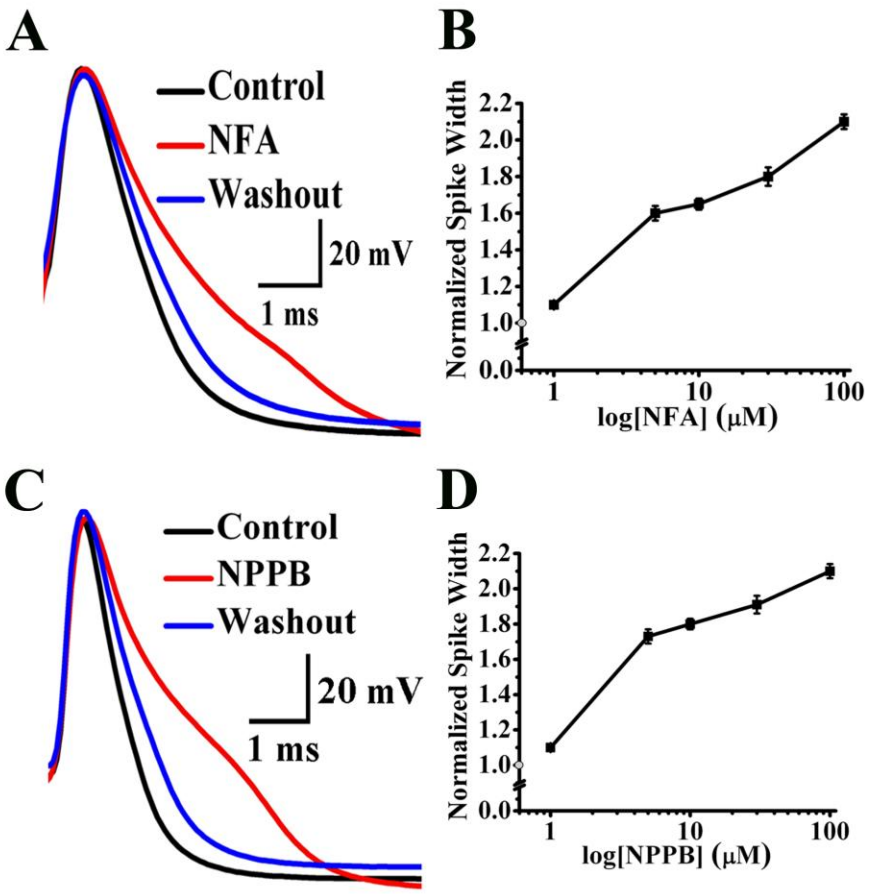
A
Control
NFA
Washout
20 mV
1 ms
B
Normalized Spike Width
2.2
2.0
1.8
1.6
1.4
1.2
1.0
0.0
1
10
100
log[NFA] (μM)
C
Control
NPPB
Washout
20 mV
1 ms
D
Normalized Spike Width
2.2
2.0
1.8
1.6
1.4
1.2
1.0
0.0
1
10
100
log[NPPB] (μM)

Figure 1. The action potential in hippocampal pyramidal neurons is broadened by CaCC blockers

(A) Blocking CaCC with NFA (red) slows the action potential repolarization compared to action potentials prior to NFA application (control, black) and after washout of NFA (blue).

(B) NFA dose-dependently increases the width of action potential (measured at 1/3 total spike height) (IC_{50} < 5 μM, n = 6).

(C-D) A second CaCC blocker, NPPB, also slows action potential repolarization (control, black, NPPB, red, washout, blue) in a dose-dependent manner (IC_{50} < 5 μM, n = 5).

Figure 2

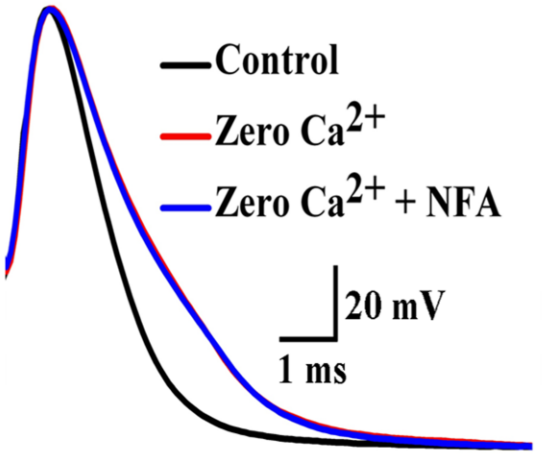

Figure 2. Removing external Ca^{2+} causes action potential broadening and occludes the NFA effect on action potential broadening (103 ± 2.7 %, n = 8 , p = 0.4), suggesting that the NFA effect on the action potential duration is due to a block of Ca^{2+}-activated Cl^- channels.

Figure 3

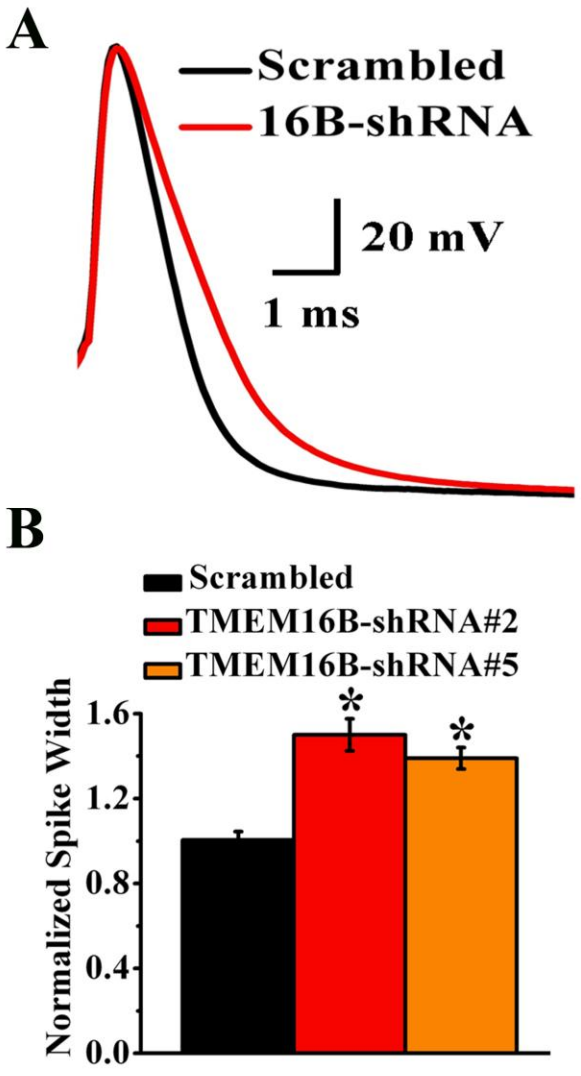
A
Scrambled
16B-shRNA
20 mV
1 ms
B
Scrambled
TMEM16B-shRNA#2
TMEM16B-shRNA#5
Normalized Spike Width
1.6
1.2
0.8
0.4
0.0
*
*

Figure 3. The action potential in hippocampal pyramidal neurons is broadened by shRNA knockdown of TMEM16B

(A-B) TMEM16B shRNA knockdown broadens action potential waveform (red and orange) as compared to scrambled RNA control (black). The TMEM16B knockdown by two different shRNA, #2 (red) and #5 (orange), slows the action potential repolarization by 50 ± 7.6% and 40 ± 5.2%, respectively (scrambled, $n = 11$, shRNA #2, $n = 9$, $p < 0.001$, shRNA #5, $n = 7$, $p < 0.001$, 12 days after infection).

Figure 4

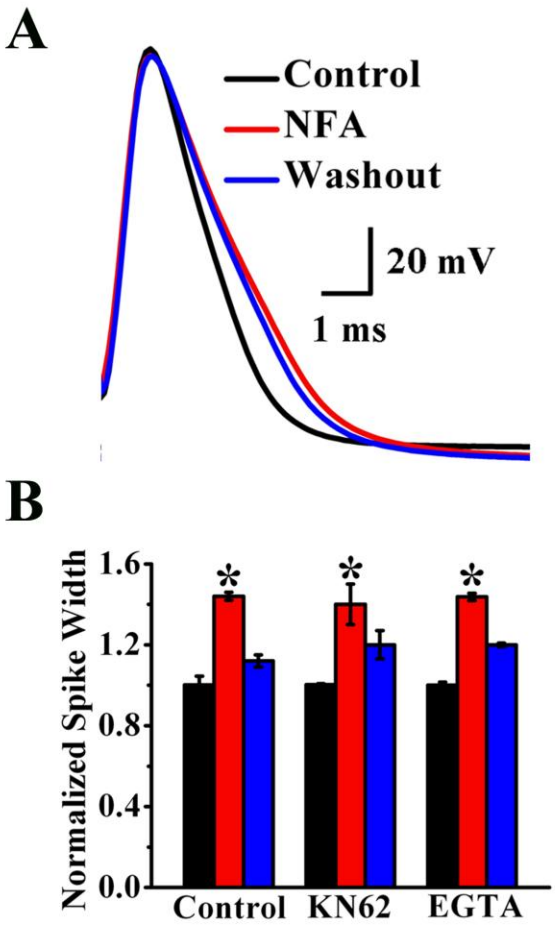
A
Control
NFA
Washout
20 mV
1 ms
B
Normalized Spike Width
1.6
1.2
0.8
0.4
0.0
*
*
*
Control
KN62
EGTA

Figure 4. CaCC shortens the duration of action potentials recorded in CA1 pyramidal neurons in acute slices

(A) Increase of action potential width by CaCC blocker is observed in CA1 pyramidal neurons in acute slice (P14-21) (control, black, 2.70 ± 0.01 ms, NFA, red, 3.91 ± 0.02 ms, $p < 0.05$, $n = 10$).

(B) The broadening effect is still observed in the presence of CaMKII blocker, KN62, suggesting that CaCC is activated by Ca^{2+}, not CaMKII (KN62, control, black, 2.53 ± 0.02 ms, NFA, red, 3.52 ± 0.03 ms, $p < 0.005$, $n = 9$). The broadening effect persists in the presence of 10 mM EGTA, suggesting that CaCCs and voltage-gated Ca^{2+} channels are close enough in distance that the slower Ca^{2+} chelator EGTA fails to prevent CaCCs from contributing to spike repolarization (EGTA, control, black, 2.71 ± 0.04 ms, NFA, red, 3.88 ± 0.04 ms, $p < 0.001$, $n = 5$).

Figure 5

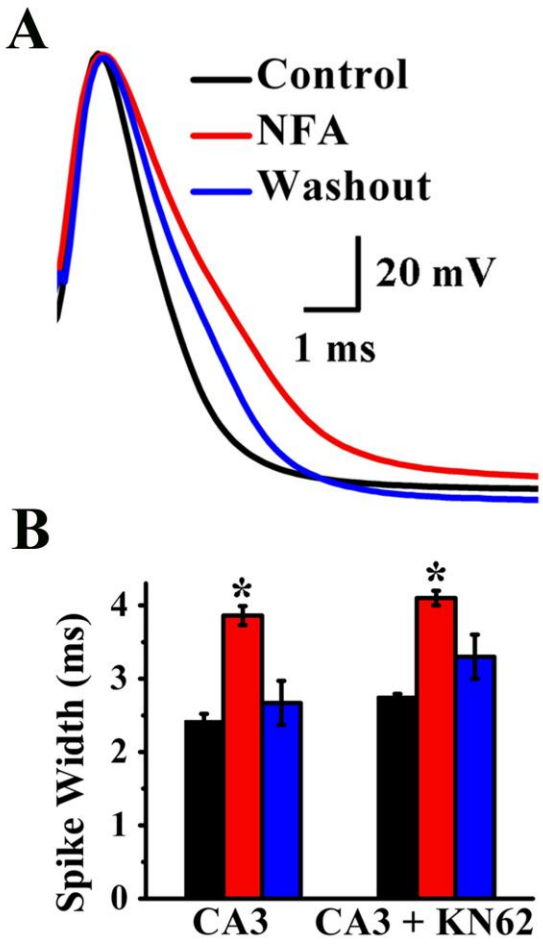
A
Control
NFA
Washout
20 mV
1 ms
B
Spike Width (ms)
0
1
2
3
4
*
*
CA3
CA3 + KN62

Figure 5. CaCC shortens the duration of action potentials recorded in CA3 pyramidal neurons in acute slices

(A-B) NFA increases the duration of action potential in CA3 pyramidal neurons in acute slices (P14-21), as evident from superimposed traces (A) and the bar graph (B), in the absence of KN62 (left, control, black, 2.43 ± 0.09 ms, NFA, red, 3.86 ± 0.13 ms) ($p < 0.005$, $n = 10$) and in the presence of the CaMKII inhibitor (right, control, black, 2.75 ± 0.024 ms, NFA, red, 4.12 ± 0.04 ms) ($p < 0.005$, $n = 11$).

Chapter 4 CaCC exerts action postsynaptically

Having found that CaCC facilitates repolarization of the action potential recorded from the soma of CA3 pyramidal neurons in acute slices, we next asked whether CaCC also affects action potential duration in their axon terminals. If so, CaCC blocker application should result in longer depolarization of the nerve terminal and therefore an increase in transmitter release from the CA3 axon terminals that form synaptic contacts with CA1 pyramidal neurons.

To approach this question, we first performed field recording of the pharmacologically isolated AMPA-fEPSP from the dendritic field of CA1 pyramidal neurons induced by stimulating Shaffer collateral axons ten times at 10 Hz (Figure 1A). As evident from the sample traces from the sixth of the ten AMPA-fEPSPs before (black) and after NFA (red) application, followed with CNQX (blue) treatment at the end of the experiment to verify that AMPA receptors mediate the fEPSPs recorded, NFA did not significantly alter the AMPA-fEPSPs (106 ± 8.4%, n = 7, p = 0.8) suggesting that CaCC exerts no effect on transmitter release (Figure 1B).

Not only was there no effect of NFA on AMPA-fEPSP, NFA also did not alter the pharmacologically isolated NMDA-EPSCs recorded from CA1 pyramidal neurons via whole-cell voltage-clamp in external solutions lacking Mg^{2+} to facilitate NMDA receptor activation and 10 mM internal Cl^- (E_{Cl} is -64 mV and holding potential is -65 mV) (101 ± 3.1%, n = 5, p = 0.2, Figure 2A). These experiments combined demonstrate that blocking CaCC alters the spike waveform in the soma without altering transmitter release,

indicating that functional CaCCs reside in somatodendritic regions but not the nerve terminals of CA3 pyramidal neurons.

Ca^{2+} flux through NMDA receptors (NMDA-R) activates CaCCs

Because activating NMDA-Rs on the dendrites also lets in Ca^{2+}, we asked whether CaCCs are present near NMDA-Rs to be activated during synaptic responses. To maximize the chance of detecting CaCC activation during NMDA-EPSC, we removed Mg^{2+} block of NMDA-R and increased Ca^{2+} influx through NMDA-Rs by replacing external Mg^{2+} with Ca^{2+} so that the Mg^{2+} concentration is 0 instead of 1.3 mM and that the external Ca^{2+} concentration is 4 mM instead of 2.5 mM.

We also experimentally increased the driving force for Cl^- ions by holding the cell at -65 mV and including 130 mM Cl^- in the whole-cell patch pipet solution ($E_{Cl} \sim 0$ mV, 65 mV driving force) so that CaCC activation would result in Cl^- efflux (inward current) hence an enhancement of the NMDA-EPSC recorded from CA1 pyramidal neurons in acute slices (P14-21) in response to Schaffer collateral stimulation every 20 seconds.

As shown in Figure 2B, superimposed average traces of five NMDA-EPSCs at the end of 5 minutes in control solution (black), end of 8 minutes in NFA (red), or end of the experiment in APV (blue) reveals that NFA (red) block of CaCC reduced the NMDA-EPSC by 28 ± 4.3 % ($p < 0.05$, $n = 10$), suggesting that CaCC is in the vicinity of NMDA-Rs to be activated by the Ca^{2+} influx through NMDA-Rs.

Importantly, when 10 mM of BAPTA, a fast Ca^{2+} chelator, is included in the 130 mM Cl^- internal solution in the patch pipet, NFA no longer had any effect (100 ± 1.4%, $n = 10$, $p = 0.13$, Figure 3A), indicating that chelating Ca^{2+} that enters through NMDA

receptors with BAPTA is sufficient to prevent CaCC activation. The internal BAPTA control further demonstrates that the NFA treatment has no presynaptic effect on transmitter release, consistent with the observation that NFA had no effect on NMDA-EPSC when pipette solution contained 10 mM Cl^- (Figure 3A).

In contrast to this, when we included 10 mM EGTA, a slower Ca^{2+} chelator, in a 130 mM Cl^-_{in} pipet solution, NFA still reduced NMDA-EPSC by 32 ± 9% ($p < 0.01$, $n = 5$, Figure 3B). As summarized in the histogram (Figure 3C), Ca^{2+} influx through NMDA-Rs is capable of activating CaCC, as revealed in conditions with elevated (130 mM) internal Cl^- level, and CaCCs are close enough to NMDA-Rs so that the slower Ca^{2+} chelator EGTA, but not the fast Ca^{2+} chelator BAPTA, allows CaCCs to activate and contribute to NMDA-EPSCs.

Figure 1

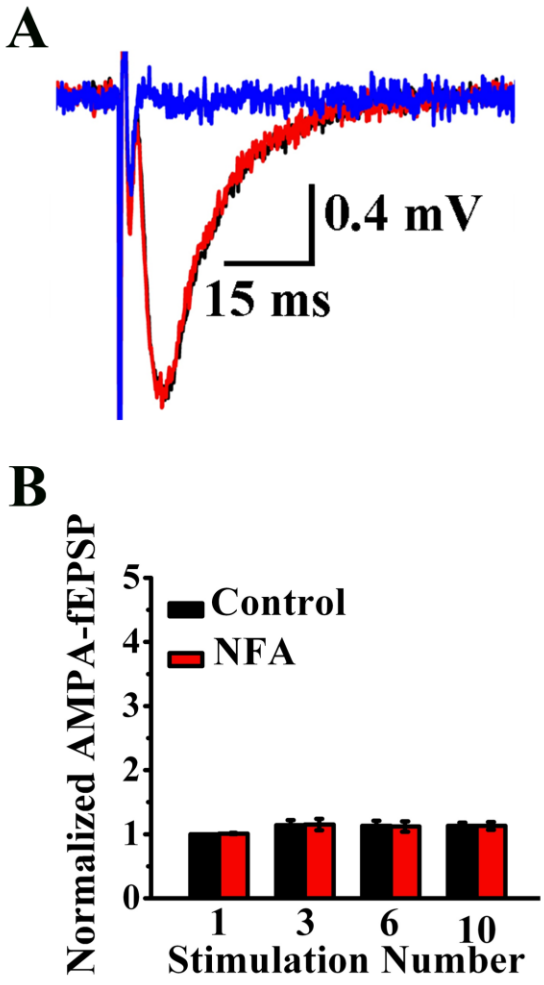
A
0.4 mV
15 ms
B
Normalized AMPA-fEPSP
Control
NFA
0
1
2
3
4
5
1
3
6
10
Stimulation Number

Figure 1. CaCC shortens the duration of action potentials recorded in CA3 pyramidal neurons, but does not affect transmitter release from their axon terminals upon stimulation of Schaffer collateral axons

(A-B) NFA (red) did not significantly alter the AMPA-fEPSPs (control, black) induced by 10 nerve stimuli at 10 Hz and monitored via field recording, suggesting that CaCC exerts no effect on transmitter release (sample 6^{th} response, $n = 7$, $p = 0.8$). Blue, 20 µM CNQX applied at the end of the experiment.

Figure 2

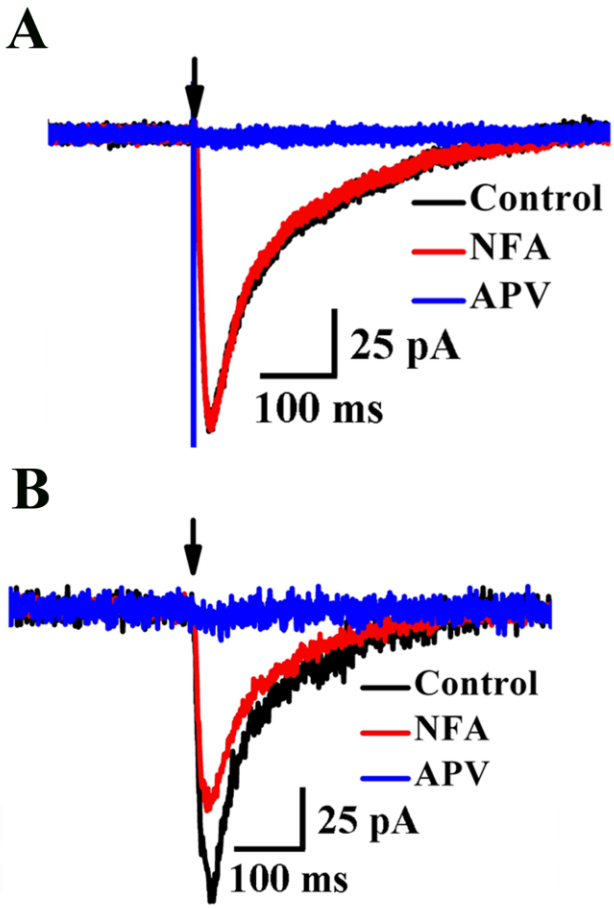

Figure 2. CaCC can be activated via Ca^{2+} flux through NMDA-Rs

(A) When there is close to no driving force for Cl^- (E_{Cl} = -64 mV with 10 Cl^-_{in}, holding potential -65 mV), NFA (red) did not significantly alter NMDA-EPSC (control, black), suggesting that NFA block of CaCC has no effect on transmitter release (n = 5, p = 0.2). Blue, 50 µM APV applied at the end of the experiment.

(B) When CaCC activation is maximized experimentally by increasing the driving force for Cl^- (E_{Cl} = 0 mV with 130Cl^-_{in}, 65 mV driving force at holding potential of -65 mV) and removing Mg^{2+} block of NMDA-Rs by using a zero-Mg^{2+} / 4 mM Ca^{2+} external solution, NFA (red) reduces NMDA-EPSC (control, black) by 28 ± 4.3% ($p < 0.05$, n = 10). Blue, 50 µM APV applied at the end of the experiment.

Figure 3

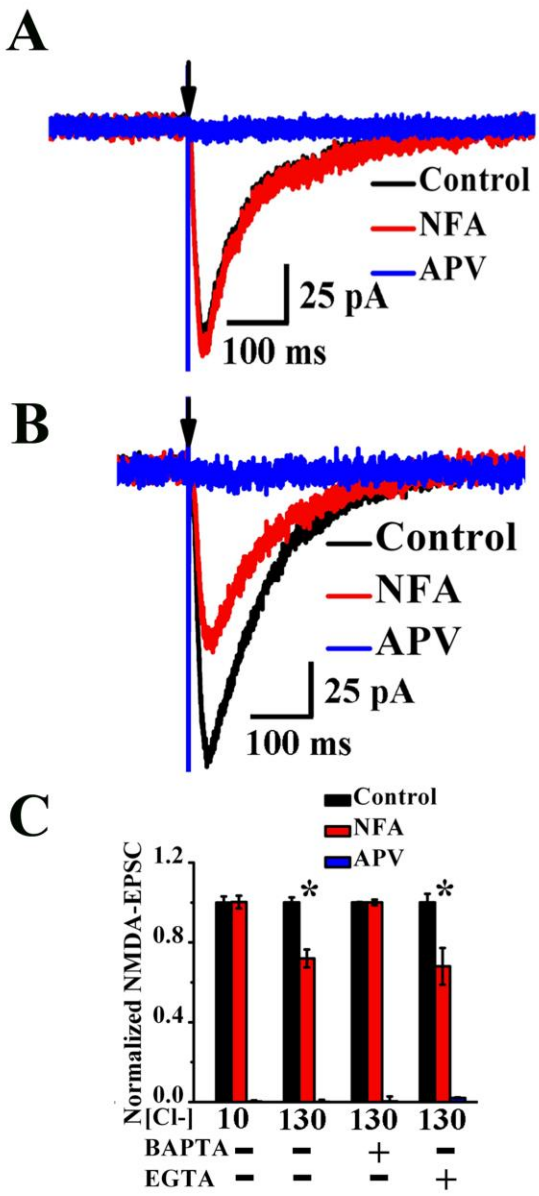
A
Control
NFA
APV
25 pA
100 ms
B
Control
NFA
APV
25 pA
100 ms
C
Control
NFA
APV
Normalized NMDA-EPSC
1.2
0.8
0.4
0.0
*
*
[Cl-] 10 130 130 130
BAPTA - - + -
EGTA - - - +

Figure 3. CaCC is in close vicinity of NMDA-Rs

(A) Chelating internal Ca^{2+} by including 10 mM BAPTA in a 130 mM Cl^-_{in} pipet solution eliminates the effect of NFA on NMDA-EPSC (black, control, red, NFA**,** blue, 50 µM APV, n = 10, p = 0.13), indicating that the NFA effect is due to a block of CaCC.

(B) With 10 mM EGTA, a slow Ca^{2+} chelator, included in a 130 mM Cl^-_{in} pipet solution, NFA (red) reduces NMDA-EPSC (control, black) by 32 ± 9 % ($p < 0.01$, n = 5). Blue, 50 µM APV applied at the end of the experiment.

(C) CaCC contributes to NMDA-EPSC when there is maximal driving force for Cl^- (130 mM Cl^-_{in}, E_{Cl} = 0 mV, $p < 0.05$, n= 10) and when there is Ca^{2+} influx through NMDA-Rs. Unlike BAPTA, which quickly chelates Ca^{2+} thereby prevents both CaCC activation and NFA effect on NMDA-EPSC, the slow Ca^{2+} chelator EGTA has no effect, suggesting that the CaCCs are in the close vicinity of NMDA-Rs.

Chapter 5 CaCC acts as a brake during excitatory synaptic responses

To explore the physiological contribution of CaCCs to synaptic responses, we stimulated Schaffer collateral at 100-200 microns from the CA1 pyramidal cell body layer every 30 seconds and performed whole cell recording from CA1 pyramidal neuron soma using physiological solution with the normal complement of 2.5 mM Ca^{2+} and 1.3 mM Mg^{2+} plus picrotoxin to block $GABA_A$ receptors. As shown in Figure 1A, NFA block of CaCC increased the EPSP amplitude (156 ± 2.9%, n = 11, $p < 0.001$), suggesting that CaCC normally acts as a brake of the excitatory synaptic potential (Figure 1B).

To explore the physiological contribution of CaCCs to the NMDA-R mediated synaptic responses, first we stimulated Schaffer collateral at 100-200 microns from the CA1 pyramidal cell body layer at 10 Hz and performed field recording of the pharmacologically isolated NMDA-fEPSP in the dendritic field of CA1 pyramidal neurons, using physiological solution with the normal complement of 2.5 mM Ca^{2+} and 1.3 mM Mg^{2+} plus CNQX to block AMPA-Rs and picrotoxin to block $GABA_A$ receptors.

During a train of nerve stimulation, NMDA-fEPSP gradually increased in size (Figure 2A, control, black). Bath application of NFA (red) increased the 3^{rd}, 6^{th}, and 10^{th} (3^{rd}, 138.4 ± 1.5 %, $p < 0.01$, 6^{th}, 145 ± 6.6 %, $p < 0.01$, 10^{th} 140 ± 6.4 %, $p < 0.01$, n = 8), but not the 1^{st} NMDA-fEPSP (105 ± 0.5 %, p = 0.8, n = 8) (Figure 2B), suggesting that only when there is consecutive synaptic responses to cause sufficient Ca^{2+} build-up for CaCC activation does NFA exert an effect on the synaptic response. This result suggests that CaCC normally acts as a brake on NMDA-R mediated synaptic potential.

To further examine the impact of CaCC activity on NMDA-R mediated synaptic potentials as they summate in a 10 Hz train to induce action potential generation, we recorded the pharmacologically isolated NMDA-EPSP in whole-cell current-clamp mode from CA1 pyramidal neurons while stimulating Schaffer collateral axons at 10 Hz, asking whether CaCC plays a role in NMDA-EPSP spike coupling.

As shown in Figure 3A, with 10 mM internal Cl^- (E_{Cl} = - 65 mV) the CaCC blocker NFA enhanced NMDA-EPSP spike coupling (control, black, first spike initiated at the 8^{th} stimulus; NFA, red, first spike initiated at the 4^{th} stimulus; APV, blue). Given the same stimulus strength, in control solution the NMDA-EPSPs transition to spiking ("EPSP-spike coupling") took place much later during a 10Hz train of synaptic responses (first spike occurring most frequently at the 10^{th} synaptic response) than when CaCC is blocked by NFA (first spike occurring most frequently at the 4^{th} or 5^{th} responses).

Accordingly the average latency to first spike (in seconds) was significantly reduced by NFA: control, 1.14 ± 0.01, NFA, 0.57 ± 0.02 ($n = 10$, $p < 0.001$, Figure 3B). And the average number of spikes per train (in spikes) was increased: control, 1.12 ± 0.05, NFA, 2.42 ± 0.2 ($n = 10$, $p < 0.001$). Thus, under the physiological condition with 10 mM internal Cl^- and E_{Cl} of - 65 mV (Cl^- channel activity is inhibitory), NFA shortens the latency to first spike and increases the average number of spikes per train.

The dependence of the CaCC function on the Cl^- ion concentration gradient was further illustrated by elevating the internal Cl^- level to 130 mM (E_{Cl} = 0 mV) so that Cl^- channel activity would be excitatory. We found that NFA delayed spike initiation and increased the average latency to first spike (in seconds): control, 0.35 ± 0.02, NFA, 0.77 ± 0.09 ($n = 10$, $p < 0.001$) (Figures 4A and 4B). NFA also reduced the average number

of spikes generated per train of 10 stimuli at 10 Hz (Figures 4A and 4B, control, black; NFA, red; APV, blue): control, 1.85 ± 0.22, NFA, 0.35 ± 0.13 ($n = 10$, $p < 0.001$). Thus, whereas CaCC normally acts as an inhibitory brake on NMDA-EPSP to spike coupling, elevating internal Cl^- concentration during neuronal activity or dysfunction could cause CaCC to provide positive feedback and enhance excitation.

Figure 1

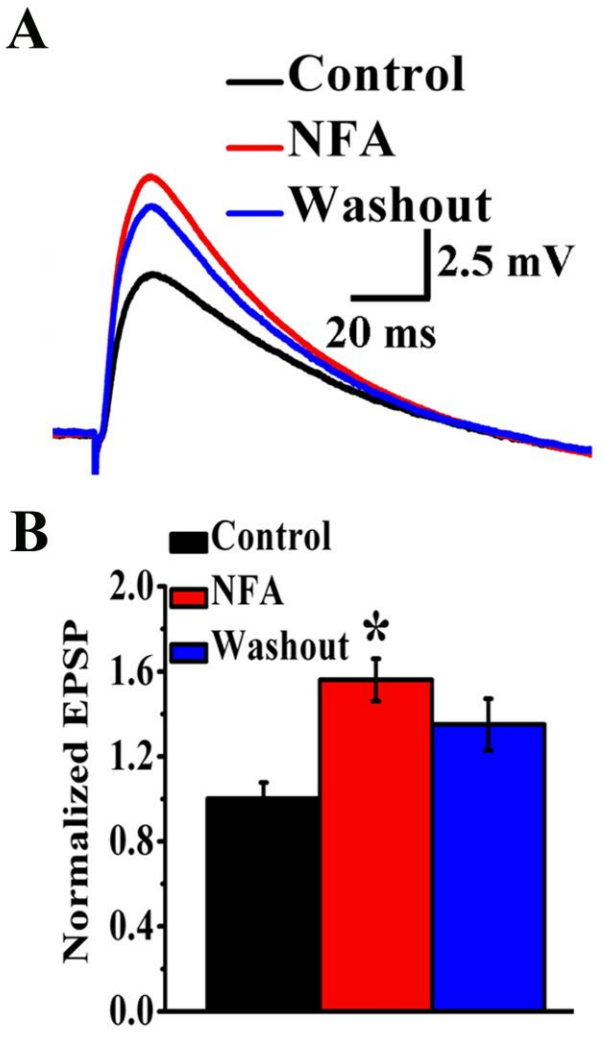
A
Control
NFA
Washout
2.5 mV
20 ms
B
Control
NFA
Washout
*
Normalized EPSP
2.0
1.6
1.2
0.8
0.4
0.0

Figure 1. CaCC activation by Ca^{2+} influx through NMDA-R provides a brake to the excitatory synaptic response

(A-B) Blocking CaCC with NFA (red) increases synaptic potential amplitude by 56 ± 2% (EPSP recorded by stimulating Schaffer collateral axons every 30 seconds) (control, black, blue, washout, $n = 11$, $p < 0.001$).

Figure 2

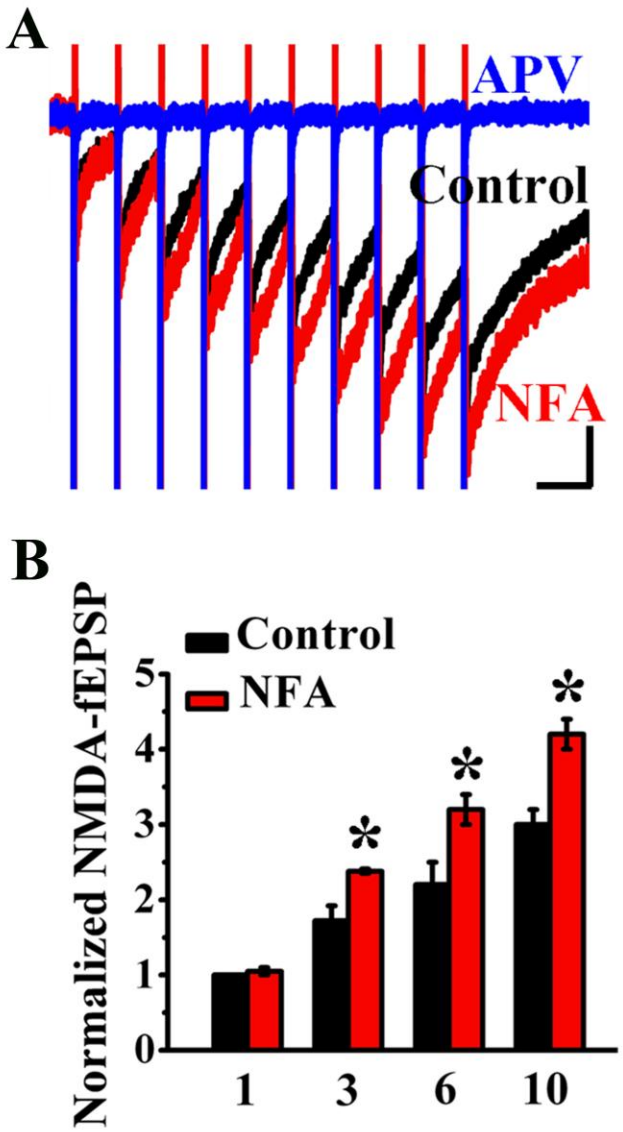
A
APV
Control
NFA
B
Normalized NMDA-fEPSP
Control
NFA
0
1
2
3
4
5
1
3
6
10
*
*
*

Figure 2. CaCC activation by Ca^{2+} influx through NMDA-R provides in turn dampens NMDA-R mediated synaptic response

(A) NFA has progressively stronger effect on NMDA-fEPSP due to a train of 10 stimuli at 10 Hz delivered to Schaffer collateral axons.

(B) Bar graphs of the field recordings showing that NFA increases the 3^{rd}, 6^{th}, and 10^{th} ($n = 8$, $p < 0.01$) but not the 1^{st} NMDA-fEPSP ($n = 8$, $p = 0.8$). Black, control, red, NFA, blue, 50 μM APV.

Figure 3

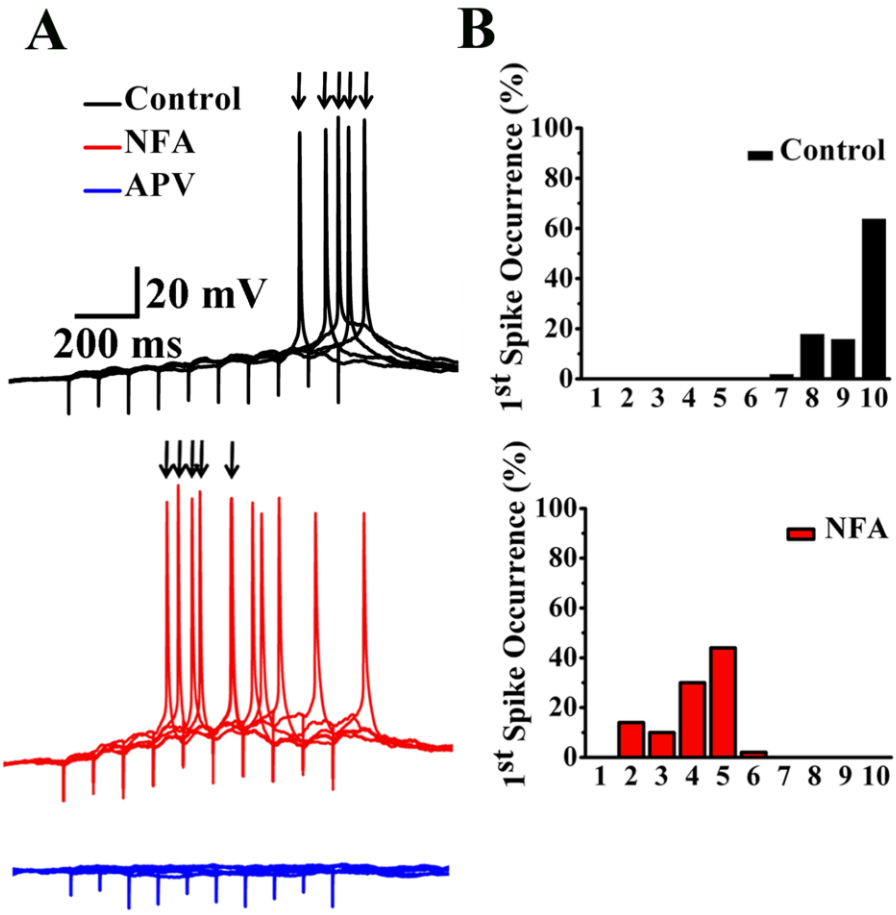
A
B
Control
NFA
APV
20 mV
200 ms
1st Spike Occurrence (%)
Control
NFA
1 2 3 4 5 6 7 8 9 10
0
20
40
60
80
100

Figure 3. CaCC activation by Ca^{2+} influx through NMDA-R provides a brake to the excitatory synaptic response when internal Cl^- is low and Cl^- activity is inhibitory

(A) With E_{Cl} = -65 mV (10 mM Cl^-_{in}), compared to control (black) the CaCC blocker NFA enhances NMDA-EPSP spike coupling (red). Blue, 50 µM APV applied at the end of the experiment. Shown are 5 superimposed sweeps with each of the 5 arrows indicating first spike in each sweep.

(B) With E_{Cl} = -65 mV (10 mM Cl^-_{in}) NFA (red) shortens the latency to first spike and increases the average number of spikes per train. Histogram quantifies the occurrence of the first spike in the responses to 10 stimuli at 10 Hz. Average latency (in seconds): control 1.14 $\pm$ 0.01, NFA 0.57 $\pm$ 0.02 ($n = 10$, $p < 0.001$). Average number of spikes per train (in spikes): control 1.12 $\pm$ 0.05, NFA 2.42 $\pm$ 0.2 ($n = 10$, $p < 0.001$).

Figure 4

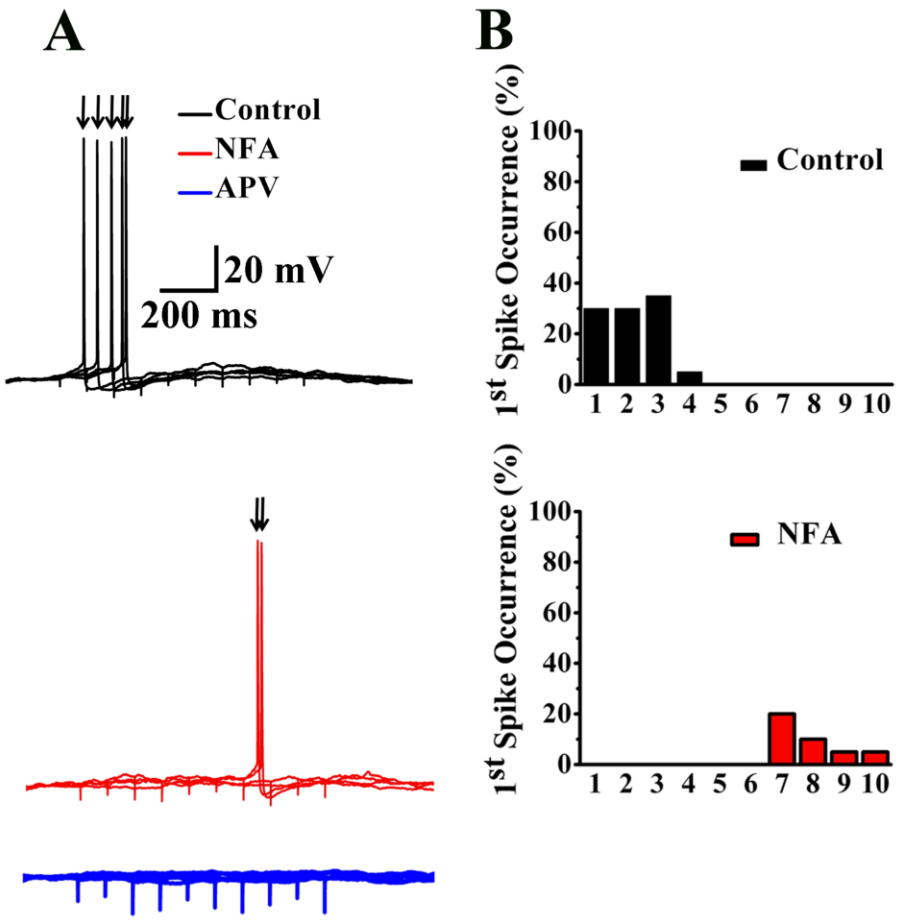
A
Control
NFA
APV
20 mV
200 ms
B
1st Spike Occurrence (%)
Control
NFA
1 2 3 4 5 6 7 8 9 10

Figure 4. CaCC activation by Ca^{2+} influx through NMDA-R enhances the excitatory synaptic response when internal Cl^- is high and Cl^- activity is excitatory

(A) With E_{Cl} = 0 mV (130 mM Cl^-_{in}), compared to control (black) the CaCC blocker NFA reduces NMDA-EPSP spike coupling (red). Blue, 50 µM APV applied at the end of the experiment. Shown are 5 superimposed sweeps with each of the 5 arrows indicating first spike in each sweep.

(B) With E_{Cl} = 0 mV (130 mM Cl^-_{in}), blocking CaCC with NFA (red) increases the latency to first spike and decreases the average number of spikes per train. Histogram quantifies the occurrence of the first spike in the responses to 10 Hz stimuli. Average latency (in seconds): control, 0.35 $\pm$ 0.02, NFA, 0.77 $\pm$ 0.09 (n = 10, $p < 0.001$). Average number of spikes per train (in spikes): control, 1.85 $\pm$ 0.22, NFA, 0.35 $\pm$ 0.13 (n =10, $p < 0.001$).

Chapter 6 Conclusions and Discussions

This is the first study to document the existence and physiological functions of Ca^{2+} activated Cl^- channels (CaCCs) in hippocampal pyramidal neurons, one of the most extensively characterized central neuronal type both because of its important involvement in learning and memory and because of its favorable anatomical organization that facilitates cellular analyses of neuronal physiology. In this study, we first show that hippocampal pyramidal neurons have functional CaCCs, and their function depend on – out of two members of the TMEM16 family that have recently been found to encode CaCCs (Caputo et al., 2008; Pifferi et al., 2009; Schroeder et al., 2008; Yang et al., 2008) – the expression of TMEM16B but not TMEM16A. We have further examined the physiological roles of CaCCs in these hippocampal neurons, as summarized below.

Our conclusion, that hippocampal pyramidal neurons express CaCCs, is based on the following findings: (1) Activation of voltage-gated Ca^{2+} channels induces a slow tail current that reverses at E_{Cl}, the Cl^- equilibrium potential. Moreover, its reversal potential shifts, with a slope of -58 mV, in accordance with the predicted changes of E_{Cl} according to the Nernst equation as the Cl^- concentration gradient across the membrane is experimentally altered. (2) This Cl^- current is dependent on Ca^{2+} for activation for the following reasons. First, the tail current amplitude correlates with the Ca^{2+} influx, increasing in size with depolarization above the threshold for Ca^{2+} channel activation and then decreasing in size with further depolarization towards E_{Ca} when Ca^{2+} influx decreases due to the diminishing driving force. Second, the tail current increases in amplitude with lengthened depolarization at a voltage with maximal driving force for

Ca^{2+} influx, but not with lengthened depolarization that is close to E_{Ca}. Third, the tail current is absent when external Ca^{2+} is replaced with Ba^{2+} or when the internal Ca^{2+} is chelated by 10 mM BAPTA. (3) The tail current is blocked by two structurally distinct CaCC blockers, NFA and NPPB. (4) This tail current is greatly reduced by shRNA knockdown of TMEM16B, which is known to encode a CaCC. Whereas the CLC-3 voltage-gated Cl^- channels that require CaMKII for activation have been found in immature hippocampal neurons (Wang et al., 2006), we found spike broadening by CaCC blockers in the presence as well as in the absence of the CaMKII inhibitor KN62. Thus, the hippocampal CaCC control of spike waveform is attributable to TMEM16B, but not CLC-3.

Given the precedence of BK channels which are activated during an action potential by Ca^{2+} influx through voltage-gated Ca^{2+} channels (Adams et al., 1982; Lancaster and Nicoll, 1987; Storm, 1987a, b), the finding that activation of voltage-gated Ca^{2+} channels leads to the opening of CaCCs prompted us to explore the possibility of CaCC modulation of action potential waveform. Our finding that action potential is broadened in hippocampal pyramidal neurons treated with either of the CaCC blockers, NFA or NPPB, or shRNA knockdown of TMEM16B, reveals that hippocampal CaCC shortens action potential duration. This CaCC modulation of the waveform of action potentials recorded from the hippocampal pyramidal neuron soma is similar to the action of the BK type of Ca^{2+}-activated K^+ channels. Interestingly, whereas BK channels also regulate the extent of transmitter release most likely due to their control of the duration of action potentials in the nerve terminal, blocking CaCC channels does not affect

transmitter release, indicating a paucity of active CaCCs in the CA3 pyramidal neuron axon terminals.

Our study further reveals that, in addition to Ca^{2+} influx through voltage-gated Ca^{2+} channels, Ca^{2+} influx through NMDA-Rs also activates CaCCs. Indeed, both whole-cell patch-clamp recordings and field recordings provide evidence that hippocampal CaCC activity modifies NMDA-EPSC and brakes NMDA-R mediated synaptic responses, analogous to the actions of the SK type of Ca^{2+}-activated K^+ channels. These findings suggest that CaCCs in somatodendritic regions of hippocampal pyramidal neurons are involved in adjusting the extent of synaptic excitation and controlling the waveform of the action potential.

How could CaCC in hippocampal neurons have escaped notice for so long? Cation channels are the focus of extensive analyses of action potentials in hippocampal pyramidal neurons, from *in vivo* recordings half a century ago (Kandel and Spencer, 1961) to recent studies of hippocampal slices and cultured neurons (Bean, 2007). Involvement of Cl^- channels was deemed unlikely early on because impaling neurons with KCl-filled electrodes leads to a reversal of the inhibitory synaptic potentials without any obvious alteration of the action potential when compared to action potentials recorded from neurons impaled with sharp electrodes containing K acetate (Storm, 1987a). By now, we have learned that different Cl^- channels differ in their abilities to distinguish between Cl^- and other anions. Indeed, whereas the inhibitory synaptic potential may be affected by loading CA1 neurons with Cl^- but not acetate because $GABA_A$ receptors allow Cl^- but not acetate ions to go through, CaCCs permeate anions

that are much larger than acetate as well as Cl^- (Bormann et al., 1987; Hartzell et al., 2005).

Possible physiological implications of CaCC modulation of action potential duration

Controlling action potential duration in different locations of a neuron has different physiological consequences. At the axon terminal, the spike duration dictates the amount of Ca^{2+} influx hence the amount of transmitter released (Hu et al., 2001; Lingle et al., 1996; Petersen and Maruyama, 1984; Raffaelli et al., 2004; Robitaille et al., 1993). In the somatodendritic region, the spike waveform along with the underlying profile of ion channel activities determines the firing pattern. We found that CaCCs control the duration of action potentials in the somatodendritic region but not the axon terminals of CA3 pyramidal neurons. This suggests that modulation of CaCC activity would impact the firing pattern – important for conveying neuronal signals both quantitatively in the number of spikes and qualitatively in the temporal arrangement of these spikes without impacting the amount of transmitter released upon the arrival of each action potential at the axon terminal.

The surprising finding that CaCC modulates action potential duration in the somatodendritic region without impacting transmitter release provides one more indication that the spike waveform is likely not uniform throughout the neuron. Indeed, Geiger and Jonas have shown that action potentials recorded from the axon terminal differ significantly in waveform from those recorded in the neuronal soma due to differential distribution of voltage-gated K^+ channels (Geiger and Jonas, 2000).

What might be the physiological impact of CaCC modulation of action potential in the somatodendritic region? Given that the CaCCs are activated by Ca^{2+} influx through NMDA receptors that have been activated by synaptic release of glutamate, CaCC likely exerts its influence over excitability in the somatodendritic region where an altered spike waveform impacts neuronal signaling in at least two possible ways: firing pattern and coincidence detection.

It is well known that changing action potential duration can alter firing pattern, as in the case of BK channels (Madison and Nicoll, 1984; Shao et al., 1999), due to the activation and inactivation profiles of multiple ion channels. Not only does the number of action potentials generated during a barrage of synaptic activities dictate the strength of the signal, the message conveyed also depends critically on the temporal pattern of spike firing. We have found that reducing CaCC activity could facilitate the NMDA-EPSP spike coupling, causing a short train of synaptic activities to initiate a burst of action potentials instead of a single spike, indicating that CaCC modulation could adjust neuronal signaling both quantitatively and qualitatively.

Action potential can back-propagate into the dendrite tree of hippocampal pyramidal neurons (Hoffman et al., 1997; Migliore et al., 1999). A back-propagating action potential invading the dendritic tree provides a window of depolarization for incoming synaptic signals to summate thereby facilitating synaptic plasticity and enhancing dendritic excitability. It is well-established that the back-propagating action potential in hippocampal pyramidal neurons gradually diminishes in size as it traverses into distal dendrites, and dendritic voltage-activated K^+ channels have been found to

provide a dampening effect to restrict action potential back propagation. Whether dendritic CaCCs also play such a role is an interesting question for future study.

Adjustment of the duration of the action potential back propagating into the dendritic tree is likely to have a strong impact not only on dendritic excitability, but also on coincidence detection of synaptic inputs – the basis of synaptic plasticity. For example, back-propagation of an action potential initiated by synaptic activity can potentiate synaptic inputs arriving at the dendrites during the same time window. Moreover, the relative timing between an incoming synaptic potential and a back-propagating spike can determine whether the synapse giving rise to the synaptic potential signal is potentiated or depressed (Caporale and Dan, 2008; Dan and Poo, 2004). A broader spike provides a larger time window for coinciding with an incoming synaptic signal, thus widening the time window during which a synaptic signal can be potentiated.

CaCC as a brake on synaptic potentials

Depolarization during synaptic transmission can activate voltage-activated K^+ channels and Ca^{2+} channels. The resultant K^+ efflux either through voltage-activated K^+ channels or through the Ca^{2+}-activated SK channels hyperpolarizes the neuronal membrane to counter the excitation. Whereas such "braking" or negative feedback during synaptic activation has conventionally been attributed to voltage-activated K^+ channels and Ca^{2+}-activated K^+ channels (SK) (Fakler and Adelman, 2008), this study provides the first evidence for the involvement of Ca^{2+}-activated Cl^- channels in the negative feedback to rein in the excitatory synaptic responses mediated by NMDA-Rs.

Our field recording of the NMDA-fEPSPs induced by a 10 Hz train of nerve stimulation has revealed that blocking CaCC activity increases the size of the NMDA-fEPSPs that arise later during the train of synaptic activities. Importantly, this synaptic activity-dependent CaCC modulation effectively enhances NMDA-EPSP spike coupling so a greater number of action potentials are generated by the same train of presynaptic inputs, with a significantly reduced latency to first spike. Modulation of CaCCs via phosphorylation or other signaling processes is therefore likely to have profound impact on the fidelity of neuronal signaling.

CaCC modulation may be modified in nature due to changes in the Cl^- gradient during physiological and pathological conditions

During normal development, the Cl^- gradient of a neuron switches from higher internal Cl^- to lower internal Cl^-, shifting E_{Cl} and converting Cl^- channel activity from excitatory to inhibitory (Ben-Ari, 2002).

Whereas most of the mature neurons normally have low internal Cl^- (5-10 mM) to allow inhibitory Cl^- channel activity, extended periods of high neuronal activity or pathological conditions such as seizures and brain traumas can lead to accumulation of internal Cl^- and revert Cl^- channel activity back to an excitatory conductance as that during the development (Blaesse et al., 2009; De Koninck, 2007; Payne et al., 2003).

Notably, the susceptibility of cation-chloride co-transporters to modulation renders the Cl^- gradient a dynamic readout of neuronal activity. For example, in mature hippocampal neurons, high levels of action potential firing can alter Cl^- gradient via activity-dependent phosphorylation of KCC2, a K^+-Cl^- co-transporter that normally

extrudes Cl^- using energy derived from the K^+ gradient (set up by Na^+-K^+ ATPase), resulting in a positive shift in E_{Cl} and changing the amount of overall inhibition (Fiumelli et al., 2005; Woodin et al., 2003). Not only will this shift in Cl^- gradient reduce the inhibitory synaptic influences, activation of CaCCs intrinsic to the neuron during high levels of spike firing is expected to progressively lose their grip over the action potential duration.

Compounding the impact of increased neuronal activity, in mature neurons of epilepsy patients, an altered Cl^- gradient is known to turn Cl^- channel activity excitatory. Epilepsy patients exhibit up-regulation of NKCC1 (Cl^- accumulator) and down-regulation of KCC2 (Cl^- extruder) in the temporal lobe, resulting in a positive shift in E_{Cl} (Palma et al., 2006). In hippocampal slices, KCC2 also undergoes down-regulation after sustained interictal-like activity in zero-Mg^{2+} conditions (Rivera et al., 2004). Similar positive shift in E_{Cl} due to altered Cl^- gradient across the membrane is also seen during brain trauma, such as fluid percussion brain injury (Bonislawski et al., 2007) and *in vivo* axonal injury (Nabekura et al., 2002)**.** These impairments of Cl^- homeostasis would turn CaCC modulation into positive feedback to further exacerbate the excitotoxicity.

In addition to modulation of the cation-chloride co-transporters, neuronal activities causing accumulation of extracellular K^+ will result in accumulation of internal Cl^-. The alteration of Cl^- gradient occurs because high neuronal activity – be it physiological during heightened neuronal activity or pathological during epilepsy or head trauma − depolarizes the cell membrane and activates voltage-gated K^+ channels, leading to K^+ efflux (driven by the intrinsic gradient of high internal K^+ and low external K^+ set by Na^+-K^+ ATPase) and accumulation of K^+ in the extracellular space (Blaesse et al.,

2009). This external K^+ accumulation reduces the driving force for K^+-Cl^- co-transporters which rely on the K^+ concentration gradient for Cl^- extrusion. The resultant Cl^- accumulation inside the cell then shifts E_{Cl} to a more positive voltage, turning Cl^- conductance to become more excitatory than during normal conditions.

The fact that CaCC can be modulated not only by changing Ca^{2+} levels but also by physiological or pathological adjustment of Cl^- gradient raises exciting new questions as to how CaCC contributes to neuronal signaling under the very relevant physiological and pathological conditions that will lead to dynamic changes of Ca^{2+} and Cl^- levels in hippocampal pyramidal neurons.

EXPERIMENTAL PROCEDURES

Cultured hippocampal neurons

Hippocampi were removed from E18-20 mouse embryos, treated with trypsin and DNase for 15 min at 37°C, and followed with gentle trituration. The dissociated cells were plated at 10^5 cells/mL onto 12-mm coverslips (Warner Instrument) that were pretreated with nitric acid and precoated with poly-L-lysine (0.1 mg/ mL; Sigma-Aldrich). Neurons were plated and maintained in Neurobasal media (Invitrogen) containing B27 extract (Invitrogen) and 1 mM L-glutamine (Sigma). Cells were recorded from 14-21 days in culture.

Acute hippocampal slices

Postnatal day 14-21 C57BL6 mice were anesthetized with isoflurane and decapitated. Brains were removed and submerged in ice-cold sucrose cutting solution (mM): 50 NaCl, 2.5 KCl, 7 $MgCl_2 \cdot 6H_2O$, 0.5 $CaCl_2 \cdot 2H_2O$, 1 $NaH_2PO_4 \cdot H_2O$, 25 $NaHCO_3$, 11 glucose, 150 sucrose, pH 7.2-7.4 after equilibrated with CO_2, ~325-340 mosm. Hippocampal slices ~400 microns thick were prepared using Leica VT1000s vibratome and transferred to a holding chamber for a minimum of 1 hour before use. The holding chamber contained oxygenated (95% O_2-5% CO_2) artificial cerebral spinal fluid (ACSF): 119 NaCl, 2.5 KCl, 1.3 $MgCl_2$, 2.5 $CaCl_2$, 1 NaH_2PO_4, 26.2 $NaHCO_3$, 11 glucose, pH 7.2-7.4 after CO_2 buffering, ~ 300 mosm.

TMEM16B shRNA

Tail current and action potential recordings were performed and compared between GFP-expressing neurons from cultures infected with lentivirus containing scrambled shRNA or TMEM16B shRNA. The target sequences of 16B-shRNA #2, 16B-shRNA #5 and scramble shRNA are GCCTCCATCTTGTTTATGATT (based on shRNA clone TRCN0000127010, Open Biosystems), GCCAGTCATCTGTTTGACAAT (based on shRNA clone TRCN0000127013, Open Biosystems), and CCTAAGGTTAAGTCGCCCTCG (based on Addgene plasmid 1864) (Sarbassov et al., 2005), respectively. The shRNAs were designed and cloned into pSicoR-GFP lentiviral transfer vector as described by Dr. Tyler Jacks laboratory (http://web.mit.edu/jacks-lab/protocols/pSico.html). Lentiviruses carrying the shRNAs were packaged and concentrated at the UCSF Sandler Center Lentiviral RNAi Core.

***In situ* hybridization**

A 2.6 kb cDNA fragment complementary to mouse TMEM16B mRNA was subcloned into the pBluescript-SK- plasmid and linearized with BamHI for antisense RNA probe synthesis by T7 transcriptase. The transcribed cRNA was hydrolyzed with sodium carbonate alkaline solution at 60^{o}C for 15 min for better tissue penetration. C57BL/6 mice were deeply anesthetized and then perfused with 4% paraformaldehyde in 0.1 M PBS, pH 7.4. Brains were removed and postfixed overnight in 4% paraformaldehyde/PBS. Brains that were to be sectioned on a cryostat were placed in 30% sucrose in 0.1M PBS (0.1% DEPC treated) until the brains sank and were then embedded in Tissue Tec OCT compound and frozen on dry ice. Frozen brains were

sectioned at 20 µm on a cryostat, and sections were mounted on VWR precleaned superfrost plus slides and stored at -80°C. Slides were thawed at room temperature for 5-10 min and were then dried in a 42°C oven for 10 min. Sections were postfixed with 4% paraformaldehyde in 0.1 M PBS for 30 min and then rinsed with 0.5x SSC for 5 min. Sections were treated with Proteinase K (1.25 mg/L) for 30 min, rinsed again with 0.5x SSC for 10 min, and air dried. The sections were covered with 75 µl of prehybridization buffer (2x SSC, 25% formamide, 1% Denhardt's reagent, 10% dextran sulfate, 0.5 mg/ml heparin, 0.5 mg/ml yeast tRNA, and 0.25 mg/ml denatured salmon sperm DNA) and incubated at 42°C for 2 h. After the prehybridization, 0.5 µg of digoxigenin-cRNA probe in 75 µl of hybridization buffer was added to each section. The sections were covered with a baked coverslip and incubated overnight at 55°C in humidified box with 25% formamide/2x SSC. The next day, the coverslips were removed and sections were washed with 2x SSC/10 mM EDTA twice. The sections were treated with RNaseA for 30 min and then washed twice with 2x SSC/EDTA. The stringency wash was 0.5x SSC/10 mM EDTA at 55°C for 2 h. After that, sections were washed with 0.5x SSC. Alkaline phosphatase-conjugated anti-digoxigenin Fab fragment (1:5000) was used to detect the hybridized probes. Nitroblue-tetrazolium-chloride/5-bromo-4-chlor-indolyl-phosphate solution was applied overnight at 4°C to detect the alkaline phosphatase. Sections were then washed with 100mM Tris-HCl (pH 8.5)/1 mM EDTA three times for 10 min each. Then slides were briefly rinsed with water twice and covered with mount medium.

RT-PCR

Cultured mouse hippocampal neurons at different DIVs were harvested and total RNA was extracted with Trizol (Invitrogen). 1-2 μg total RNA was used for cDNA synthesis with SuperScript III First-Strand Synthesis System for RT-PCR (Invitrogen). Primers specific to mouse TMEM16B and TMEM16A were used for PCR amplification.

TMEM16B antibody generation and Western blot

A rabbit polyclonal antibody was generated against an extracellular epitope of mouse TMEM16B (QLKEGTQPENSQFDQE). The specificity of the antibody was tested with the exogenously expressed mouse TMEM16B-mCherry in HEK293 cells by western blot.

Endogenous TMEM16B in mouse hippocampal neurons was detected by western blot with the rabbit polyclonal antibody. Briefly, cultured hippocampal neurons were lysed in PBS/1% Triton X-100 or PBS/1% SDS for 30 min at 4°C. After centrifugation at 100,000 x g for 10 min, the supernatant were retained for SDS-PAGE gel electrophoresis. The blot was incubated 2hrs RT with primary antibodies, followed by incubation with HRP-linked secondary antibodies. The blot then was treated with ECL Plus regent (Amersham) and exposed to film. The primary antibodies were used at the following dilutions: TMEM16B 1:500, mouse anti-tubulin (sigma) 1:2000, rat anti-DsRed 1:500.

Electrophysiology

Hippocampal Cultures

Whole-cell recordings were performed on individual cultured pyramidal neurons. Pyramidal neurons were distinguishable by their relatively large size, lower input resistance (100-200 MΩ), and prominent apical dendrite. The recording pipettes were made from borosilicate glass capillaries (P-97 Sutter Instrument, 1.5 mm/0.86 mm) and pulled on the day of use (3-4 MΩ). All internal solutions have pH 7.2-7.4 and ~300 mosm. All external solutions were made fresh the day of use and adjusted to pH 7.2-7.4 and ~ 300 mosm (measured on the day of use). The bath was constantly perfused with fresh external solution at 2 mL/min throughout the recording, and all experiments were performed at room temperature. The neurons were visualized with a CCD camera (Hamamatsu). Recordings were amplified with MultiClamp 700B (Axon Instruments), and data were analyzed and plotted with Clampfit 10 and ORIGIN.

For tail current recordings in hippocampal cultured neurons, the pipettes were filled with the following (mM):

23 mM internal Cl^- solution: 10 HEPES, 0.2 EGTA, 125 Cs-gluconate, 18 CsCl, 5 TEACl. 10 mM internal Cl^- solution: 10 HEPES, 0.2 EGTA, 138 Cs-gluconate, 5 CsCl, 5 TEACl. 5 mM internal Cl^- solution: 10 HEPES, 0.2 EGTA, 140.5 Cs-gluconate, 2.5 CsCl, 2.5 TEACl. pH = 7.2-7.4, adjusted with CsOH, ~300 mosm.

Internal solution containing BAPTA for tail current recording (mM): 10 BAPTA, 10 HEPES, 0.2 EGTA, 125 Cs-gluconate, 18 CsCl, 5 TEACl, pH 7.2-7.4, ~ 300 mosm. The external bath solution for tail current recordings contained (mM unless specified) 140 NMDG-Cl, 20 HEPES, 1.3 $MgCl_2$, 2.5 $CaCl_2$, 5 4-AP, 1 μM TTX, 50 μM PTX.

A depolarization prepulse from -70 mV holding potential to 0 mV was used to elicit inward Ca^{2+} current followed by a long tail current (100s of ms before returning to baseline). For obtaining current-voltage relationship for the tail current, tail current obtained without the depolarization prepulse was subtracted from the tail current obtained with the depolarization prepulse to rid of background current. Voltage steps from -100 to -30 mV (delta 5 mV or 10 mV) were placed on the tail current region, and the subtracted tail current was plotted as function of the voltage. Reversal potential was the voltage at which the subtracted tail current changed directions.

For action potential recordings in hippocampal cultured neurons, internal solution contained (mM): 140 K-gluconate, 10 KCl, 10 HEPES, 0.2 EGTA, 4 Mg-ATP, 0.4 Na-GTP, pH 7.2-7.4, adjusted with KOH, ~ 300 mosm. ACSF (see above) was used as bath solution for action potential recordings. $CaCl_2$ was omitted for the zero Ca^{2+} experiment and replaced with $BaCl_2$ during the Ba^{2+} replacement experiment.

Acute Hippocampal Slices

Bipolar stimulating electrode was placed in *stratum radiatum* to stimulate the Schaffer collaterals (axons of CA3 neurons) and whole-cell recordings from the cell bodies of CA1 pyramidal neurons were obtained. The external bath solution was oxygenated with 95% O_2-5%CO_2 and the slices were continually perfused at 2 mL/min in room temperature. The neurons were visualized with a CCD camera (Hamamatsu). Recordings were performed with patch clamp amplifiers (MultiClamp 700B, Axon Instruments), and data were analyzed and plotted with Clampfit 10 and ORIGIN.

To record action potentials in acute slices, whole cell recordings (current-clamp mode) from CA1 and CA3 pyramidal neurons were obtained with K-gluconate based internal solution (same as that used for action potential recording from cultured neurons) and ACSF was used as the external solution (including 50 µM PTX for all recordings and additional 20 µM KN62 for the CaMKII experiment). 2 ms current injection (just suprathreshold) was used to elicit a single action potential.

To obtain field recordings, 5-10 MΩ recording pipettes were filled with ACSF and the external bath solutions contained ACSF with additional blockers of transmitter receptors. For field recording of NMDA-fEPSP, the external solution also included 50 µM PTX and 20 µM CNQX, and 50 µM D-APV was added at the end of experiment. For AMPA-fEPSP recording, the external solution also included 50 µM PTX and 50 µM D-APV, and 20 µM CNQX was added at the end of experiment. The 10 Hz stimulation was delivered with a bipolar stimulating electrode placed 100-200 microns from the recording pipette in the CA1 dendritic field.

To record whole-cell NMDA-EPSCs, 3-4 MΩ recording pipettes were filled with 130 mM Cl^-_{in} solution: 10 K-gluconate, 130 KCl, 10 HEPES, 0.2 EGTA, 4 MgATP, 0.4 Na_3GTP, pH 7.2-7.4, adjusted with KOH, ~ 300 mosm. 10 mM BAPTA was added in experiments testing whether CaCC activation via NMDA-Rs was Ca^{2+} dependent. To make the 10 mM Cl^- internal solution, K-gluconate concentration was raised from 10 mM to 130 mM and KCl concentration was reduced from 130 mM to 10 mM. A zero-Mg^{2+} ACSF (without 1.3 mM Mg^{2+} but with 4 mM $CaCl_2$) was used as the external solution in order to remove Mg^{2+} block and have Ca^{2+} flux through NMDA-R activated by stimulating Schaffer collateral axons at a holding potential of -65 mV. $GABA_A$-Cl^-

current was blocked with 50 µM PTX and the AMPA receptor contribution was removed with 20 µM CNQX. 100 µM APV was added at the end of the experiment to verify that NMDA receptors mediated the NMDA-EPSC recorded. Bipolar stimulation electrode was placed 100-200 µm from the CA1 pyramidal neuron cell body layer to deliver a stimulus lasting 0.1 msec every 30 seconds.

For whole-cell recording of NMDA-EPSPs, 3-4 MΩ recording pipettes were filled with 10 mM Cl^-_{in} solution: 130 K-gluconate, 10 KCl, 10 HEPES, 0.2 EGTA, 4 MgATP, 0.4 Na_3GTP, pH 7.2-7.4, adjusted with KOH, ~ 300 mosm. For 130 mM Cl^-_{in} experiment, 130 K-gluconate concentration was reduced from 130 mM to 10 mM and KCl concentration was raised from 10 mM to 130 mM. ACSF was used for the external solution and included 50 µM PTX to block $GABA_A$-Cl^- channels and 20 µM CNQX to remove AMPA receptor contribution. 100 µM APV was added at the end of the experiment to verify that NMDA receptors mediated the NMDA-EPSP recorded. Bipolar stimulation electrode was place 100-200 µm from the CA1 pyramidal neuron cell body layer to deliver a stimulus lasting ~ 0.1 msec every 30 seconds.

Picrotoxin (PTX), D-(-)-2-Amino-5-phosphonopentanoic acid (D-APV), tetrodotoxin (TTX), 4-aminopyridine (4AP), KN62 were purchased from Tocris (Ellisville, Missouri). Niflumic acid (NFA), 5-nitro-2-(3-phenylpropylamino)benzoic acid (NPPB), and 6-cyano-7-nitroquinoxaline-2,3-dione (CNQX) were purchased from Sigma Aldrich.

REFERENCES

Adams, P.R., Constanti, A., Brown, D.A., and Clark, R.B. (1982). Intracellular Ca^{2+} activates a fast voltage-sensitive K^{+} current in vertebrate sympathetic neurones. Nature *296*, 746-749.

Barnes, S., and Hille, B. (1989). Ionic channels of the inner segment of tiger salamander cone photoreceptors. J Gen Physiol *94*, 719-743.

Bean, B.P. (2007). The action potential in mammalian central neurons. Nat Rev Neurosci *8*, 451-465.

Ben-Ari, Y. (2002). Excitatory actions of gaba during development: the nature of the nurture. Nat Rev Neurosci *3*, 728-739.

Blaesse, P., Airaksinen, M.S., Rivera, C., and Kaila, K. (2009). Cation-chloride cotransporters and neuronal function. Neuron *61*, 820-838.

Bonislawski, D.P., Schwarzbach, E.P., and Cohen, A.S. (2007). Brain injury impairs dentate gyrus inhibitory efficacy. Neurobiol Dis *25*, 163-169.

Bormann, J., Hamill, O.P., and Sakmann, B. (1987). Mechanism of anion permeation through channels gated by glycine and gamma-aminobutyric acid in mouse cultured spinal neurones. J Physiol *385*, 243-286.

Caporale, N., and Dan, Y. (2008). Spike timing-dependent plasticity: a Hebbian learning rule. Annu Rev Neurosci *31*, 25-46.

Caputo, A., Caci, E., Ferrera, L., Pedemonte, N., Barsanti, C., Sondo, E., Pfeffer, U., Ravazzolo, R., Zegarra-Moran, O., and Galietta, L.J. (2008). TMEM16A, a membrane protein associated with calcium-dependent chloride channel activity. Science *322*, 590-594.

Dan, Y. and Poo, M.M. (2004). Spike timing-dependent plasticity of neural circuits. Neuron *44*, 23-30.

De Koninck, Y. (2007). Altered chloride homeostasis in neurological disorders: a new target. Curr Opin Pharmacol *7*, 93-99.

Fakler, B., and Adelman, J.P. (2008). Control of K(Ca) channels by calcium nano/microdomains. Neuron *59*, 873-881.

Fiumelli, H., Cancedda, L., and Poo, M.M. (2005). Modulation of GABAergic transmission by activity via postsynaptic Ca^{2+}-dependent regulation of KCC2 function. Neuron *48*, 773-786.

Frings, S., Reuter, D., and Kleene, S.J. (2000). Neuronal Ca^{2+}-activated Cl^- channels--homing in on an elusive channel species. Prog Neurobiol *60*, 247-289.

Geiger, J.R., and Jonas, P. (2000). Dynamic control of presynaptic Ca^{2+} inflow by fast-inactivating K^+ channels in hippocampal mossy fiber boutons. Neuron *28*, 927-939.

Hammond, R.S., Bond, C.T., Strassmaier, T., Ngo-Anh, T.J., Adelman, J.P., Maylie, J., and Stackman, R.W. (2006). Small-conductance Ca^{2+}-activated K^+ channel type 2 (SK2) modulates hippocampal learning, memory, and synaptic plasticity. J Neurosci *26*, 1844-1853.

Hartzell, C., Putzier, I., and Arreola, J. (2005). Calcium-activated chloride channels. Annu Rev Physiol *67*, 719-758.

Higashi, H., Tanaka, E., Inokuchi, H., and Nishi, S. (1993). Ionic mechanisms underlying the depolarizing and hyperpolarizing afterpotentials of single spike in guinea-pig cingulate cortical neurons. Neuroscience *55*, 129-138.

Hodgkin, A.L., and Huxley, A.F. (1952). Propagation of electrical signals along giant nerve fibers. Proc R Soc Lond B Biol Sci *140*, 177-183.

Hoffman, D.A., Magee, J.C., Colbert, C.M., and Johnston, D. (1997). K^+ channel regulation of signal propagation in dendrites of hippocampal pyramidal neurons. Nature *387*, 869-875.

Hu, H., Shao, L.R., Chavoshy, S., Gu, N., Trieb, M., Behrens, R., Laake, P., Pongs, O., Knaus, H.G., Ottersen, O.P., and Storm, J.F. (2001). Presynaptic Ca^{2+}-activated K^+ channels in glutamatergic hippocampal terminals and their role in spike repolarization and regulation of transmitter release. J Neurosci *21*, 9585-9597.

Huang, F., Rock, J.R., Harfe, B.D., Cheng, T., Huang, X., Jan, Y.N., and Jan, L.Y. (2009). Studies on expression and function of the TMEM16A calcium-activated chloride channel. Proc Natl Acad Sci U S A *106*, 21413-21418.

Hwang, S.J., Blair, P.J., Britton, F.C., O'Driscoll, K.E., Hennig, G., Bayguinov, Y.R., Rock, J.R., Harfe, B.D., Sanders, K.M., and Ward, S.M. (2009). Expression of anoctamin 1/TMEM16A by interstitial cells of Cajal is fundamental for slow wave activity in gastrointestinal muscles. J Physiol *587*, 4887-4904.

Kandel, E.R., and Spencer, W.A. (1961). Electrophysiology of hippocampal neurons. II. After-potentials and repetitive firing. J Neurophysiol *24*, 243-259.

Korn, S.J., Bolden, A., and Horn, R. (1991). Control of action potentials and Ca^{2+} influx by the Ca^{2+}-dependent chloride current in mouse pituitary cells. J Physiol *439*, 423-437.

Lancaster, B., and Nicoll, R.A. (1987). Properties of two calcium-activated hyperpolarizations in rat hippocampal neurones. J Physiol *389*, 187-203.
Lin, M.T., Lujan, R., Watanabe, M., Adelman, J.P., and Maylie, J. (2008). SK2 channel plasticity contributes to LTP at Schaffer collateral-CA1 synapses. Nat Neurosci *11*, 170-177.

Lingle, C.J., Solaro, C.R., Prakriya, M., and Ding, J.P. (1996). Calcium-activated potassium channels in adrenal chromaffin cells. Ion Channels *4*, 261-301.

Madison, D.V., and Nicoll, R.A. (1984). Control of the repetitive discharge of rat CA 1 pyramidal neurones in vitro. J Physiol *354*, 319-331.

Manoury, B., Tamuleviciute, A., and Tammaro, P. (2010). TMEM16A/anoctamin 1 protein mediates calcium-activated chloride currents in pulmonary arterial smooth muscle cells. J Physiol *588*, 2305-2314.

Migliore, M., Hoffman, D.A., Magee, J.C., and Johnston, D. (1999). Role of an A-type K^+ conductance in the back-propagation of action potentials in the dendrites of hippocampal pyramidal neurons. J Comput Neurosci *7*, 5-15.

Nabekura, J., Ueno, T., Okabe, A., Furuta, A., Iwaki, T., Shimizu-Okabe, C., Fukuda, A., and Akaike, N. (2002). Reduction of KCC2 expression and GABAA receptor-mediated excitation after in vivo axonal injury. J Neurosci *22*, 4412-4417.

Ngo-Anh, T.J., Bloodgood, B.L., Lin, M., Sabatini, B.L., Maylie, J., and Adelman, J.P. (2005). SK channels and NMDA receptors form a Ca2+-mediated feedback loop in dendritic spines. Nat Neurosci *8*, 642-649.

Palma, E., Amici, M., Sobrero, F., Spinelli, G., Di Angelantonio, S., Ragozzino, D., Mascia, A., Scoppetta, C., Esposito, V., Miledi, R., and Eusebi, F. (2006). Anomalous levels of Cl^- transporters in the hippocampal subiculum from temporal lobe epilepsy patients make GABA excitatory. Proc Natl Acad Sci U S A *103*, 8465-8468.

Payne, J.A., Rivera, C., Voipio, J., and Kaila, K. (2003). Cation-chloride co-transporters in neuronal communication, development and trauma. Trends Neurosci *26*, 199-206.

Petersen, O.H., and Maruyama, Y. (1984). Calcium-activated potassium channels and their role in secretion. Nature *307*, 693-696.

Pifferi, S., Dibattista, M., and Menini, A. (2009). TMEM16B induces chloride currents activated by calcium in mammalian cells. Pflugers Arch *458*, 1023-1038.

Raffaelli, G., Saviane, C., Mohajerani, M.H., Pedarzani, P., and Cherubini, E. (2004). BK potassium channels control transmitter release at CA3-CA3 synapses in the rat hippocampus. J Physiol *557*, 147-157.

Rivera, C., Voipio, J., Thomas-Crusells, J., Li, H., Emri, Z., Sipila, S., Payne, J.A., Minichiello, L., Saarma, M., and Kaila, K. (2004). Mechanism of activity-dependent downregulation of the neuron-specific K-Cl cotransporter KCC2. J Neurosci *24*, 4683-4691.

Robitaille, R., Garcia, M.L., Kaczorowski, G.J., and Charlton, M.P. (1993). Functional colocalization of calcium and calcium-gated potassium channels in control of transmitter release. Neuron *11*, 645-655.

Rock, J.R., O'Neal, W.K., Gabriel, S.E., Randell, S.H., Harfe, B.D., Boucher, R.C., and Grubb, B.R. (2009). Transmembrane protein 16A (TMEM16A) is a Ca^{2+}-regulated Cl^- secretory channel in mouse airways. J Biol Chem *284*, 14875-14880.

Romanenko, V.G., Catalan, M.A., Brown, D.A., Putzier, I., Hartzell, H.C., Marmorstein, A.D., Gonzalez-Begne, M., Rock, J.R., Harfe, B.D., and Melvin, J.E. (2010). Tmem16A encodes the Ca^{2+}-activated Cl^- channel in mouse submandibular salivary gland acinar cells. J Biol Chem *285*, 12990-13001.

Sarbassov, D.D., Guertin, D.A., Ali, S.M., and Sabatini, D.M. (2005). Phosphorylation and regulation of Akt/PKB by the rictor-mTOR complex. Science *307*, 1098-1101.

Schroeder, B.C., Cheng, T., Jan, Y.N., and Jan, L.Y. (2008). Expression cloning of TMEM16A as a calcium-activated chloride channel subunit. Cell *134*, 1019-1029.

Scott, R.H., Sutton, K.G., Griffin, A., Stapleton, S.R., and Currie, K.P. (1995). Aspects of calcium-activated chloride currents: a neuronal perspective. Pharmacol Ther *66*, 535-565.

Shao, L.R., Halvorsrud, R., Borg-Graham, L., and Storm, J.F. (1999). The role of BK-type Ca^{2+}-dependent K^+ channels in spike broadening during repetitive firing in rat hippocampal pyramidal cells. J Physiol *521 Pt 1*, 135-146.

Stackman, R.W., Hammond, R.S., Linardatos, E., Gerlach, A., Maylie, J., Adelman, J.P., and Tzounopoulos, T. (2002). Small conductance Ca^{2+}-activated K^+ channels modulate synaptic plasticity and memory encoding. J Neurosci *22*, 10163-10171.

Stephan, A.B., Shum, E.Y., Hirsh, S., Cygnar, K.D., Reisert, J., and Zhao, H. (2009). ANO2 is the cilial calcium-activated chloride channel that may mediate olfactory amplification. Proc Natl Acad Sci U S A *106*, 11776-11781.

Stohr, H., Heisig, J.B., Benz, P.M., Schoberl, S., Milenkovic, V.M., Strauss, O., Aartsen, W.M., Wijnholds, J., Weber, B.H., and Schulz, H.L. (2009). TMEM16B, a novel protein with calcium-dependent chloride channel activity, associates with a presynaptic protein complex in photoreceptor terminals. J Neurosci *29*, 6809-6818.

Storm, J.F. (1987a). Action potential repolarization and a fast after-hyperpolarization in rat hippocampal pyramidal cells. J Physiol *385*, 733-759.

Storm, J.F. (1987b). Intracellular injection of a Ca^{2+} chelator inhibits spike repolarization in hippocampal neurons. Brain Res *435*, 387-392.

Sugita, S., Tanaka, E., and North, R.A. (1993). Membrane properties and synaptic potentials of three types of neurone in rat lateral amygdala. J Physiol *460*, 705-718.

Wang, X.Q., Deriy, L.V., Foss, S., Huang, P., Lamb, F.S., Kaetzel, M.A., Bindokas, V., Marks, J.D., and Nelson, D.J. (2006). CLC-3 channels modulate excitatory synaptic transmission in hippocampal neurons. Neuron *52*, 321-333.

Woodin, M.A., Ganguly, K., and Poo, M.M. (2003). Coincident pre- and postsynaptic activity modifies GABAergic synapses by postsynaptic changes in Cl^- transporter activity. Neuron *39*, 807-820.

Yang, Y.D., Cho, H., Koo, J.Y., Tak, M.H., Cho, Y., Shim, W.S., Park, S.P., Lee, J., Lee, B., Kim, B.M., *et al.* (2008). TMEM16A confers receptor-activated calcium-dependent chloride conductance. Nature *455*, 1210-1215.

Publishing Agreement

It is the policy of the University to encourage the distribution of all theses, dissertations, and manuscripts. Copies of all UCSF theses, dissertations, and manuscripts will be routed to the library via the Graduate Division. The library will make all theses, dissertations, and manuscripts accessible to the public and will preserve these to the best of their abilities, in perpetuity.

Please sign the following statement:

I hereby grant permission to the Graduate Division of the University of California, San Francisco to release copies of my thesis, dissertation, or manuscript to the Campus Library to provide access and preservation, in whole or in part, in perpetuity.

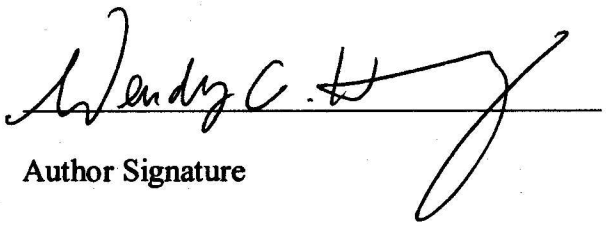

Author Signature

11/11/10

Date